PIRAEUS UNIVERSITY OF APPLIED SCIENCES

TEI OF PIRAEUS

University of Brighton

Enhanced VOF-based CFD simulations of droplet impact

Dissertation Submitted by

Konstantinos Vontas

Under Supervision of

Dr. Anastasios Georgoulas

A dissertation submitted to the Department of Mechanical Engineering of
Piraeus University of Applied Sciences
in partial fulfillment of the requirement for the degree of

Bachelor of Science
in
Mechanical Engineering

June 2016

DECLARATION

I hereby declare that this thesis is my own work and that, to the best of my knowledge and belief. It contains no material previously published or produced by another party in fulfilment, partial or otherwise, of any other degree or diploma at another University or Institution of higher learning, except where due acknowledgment is made in the text.

Konstantinos M. Vontas

1st of June 2016

I would like to dedicate this work to Almighty God, my parents Michalis and Sofia and to my sisters Marianna and Eleni

"So do not fear, for I am with you; do not dismayed, for I am your God. I will strengthen you and help you; I will uphold you with my righteous right hand".

Isaiah 41:10

Στους αγαπημένους μου γονείς Μιχάλη και Σοφία

ACKNOWLEDGMENTS

First of all, I am grateful to thank my supervisor, Senior Lecturer Dr. Anastasios Georgoulas and express him my deepest appreciation and respect, not only for his confidence in me, his willingness to share his knowledge with me and for being available at any time-any day of the week whenever I was in trouble spot, but also for his advises and help regarding my future career as Mechanical Engineer.

Second of all, I would like to thank Prof. Marco Marengo for his hospitality and for giving me the chance to join his world class research group.

Moreover, I would like to acknowledge Prof. Marengo as well as Dr. Georgoulas for trusting me and letting me use, whether Marengo's Work Station (WS) as well as the super-computing facilities of CINECA, in Bologna, Italy.

Also I would like to thank the school of Computing, Mathematics and Engineering of University of Brighton for their warm welcome.

Last but not least, I would like to thank the Professor of my home Institution TEI Piraeus, Konstantinos-Stefanos Nikas for his support and advices not only during my studies in my home Institution but also while I was an exchange student in Norway as well as in the UK. Without his contribution all these years, my studies abroad both in the past and in the future, would not have been possible.

Furthermore, I would like to acknowledge all the Professors as well as the employees of my home University, part of this work belongs to them.

To all of you …. Thank you

Nomenclature

D droplet diameter m
g gravitational acceleration m/s^2
l length of contact line m
L total length of contact line m
P, p pressure Pa
R droplet radius m
Re Reynolds number (–)
t time s
U, V velocity m/s
We Webber number (–)

Greek letters

ϑ contact angle (°)
μ dynamic viscosity kg/ms
v kinematic viscosity m^2/s
ρ density kg/m^3
σ, γ surface tension coefficient N/m

Subscripts

adv advancing
dyn dynamic
eq equilibrium
liq liquid
max maximum
0 initial condition
rec receding

CA Contact angle
CMOS Complementary metal–oxide–semiconductor
CFD Computational Fluid Dynamics
FEM Finite Element Method
VOF Volume of Fluid
CLSVOF Coupled Level Set/Volume of Fluid
DLSGM Dual-Grid Level-Set Method
CMFD computational multi-fluid dynamics
N/D No Data

TABLE OF CONTENTS

Chapter 4

Chapter 5

1.1 Overview

Droplet impact on a solid surface is an often encountered phenomenon both in nature as well as in industry. The last years many investigations have been conducted utilizing numerical simulations, laboratory experiments as well as pure theoretical studies, in order to explain droplet impact related phenomena observed in nature and furthermore in many engineering applications. Droplet impact has many practical applications in engineering, for example, in fuel injection systems where droplets from fuel sprays interact with the solid surfaces of the combustion chamber. Another application of droplet impact is cooling of hot surfaces (e.g. electronic circuits) by impingement of cold liquid droplets onto them [1]. Moreover, more recently droplet impact related investigations on ink-jet printing technology have also been conducted, for printing onto paper but also in the manufacturing process for displays, such as polymer organic light emitting diodes [2]. Droplet dynamics are not implemented only in engineering fields but it has also a lot of biological applications, such as the impact of microscopic droplets on human skin for dermatological care purposes [3].

1.2.1 Aims

The main aim of the present Final Year Project is to extensively validate an enhanced, VOF - based numerical simulation method developed in developed in the context of OpenFOAM CFD Toolbox, for the simulation of droplet impact phenomena, with literature available experimental data on droplet impact. In more detail, some specific experimental runs that are presented in the works of Pasandideh-Fard et al [4], Yokoi et al. [5], Patil et al. [6] and Bushan et al. [7] are reproduced numerically and the model predictions are compared with the corresponding experimental measurements.

Initially, three different contact angle treatments are compared with a specific experimental run from the work of Pasandideh-Fard et al. [3]. A constant contact angle treatment (already implemented in OpenFOAM from the official distribution), a dynamic contact angle treatment (already implemented in OpenFOAM from the official distribution) and Kistler's dynamic contact angle model (that has been implemented for the purposes of the present FYP as a user defined boundary condition for wall-adhesion). From this initial comparison, Kistler's model is selected since it is more close to the experimental droplet evolution.

Then after ensuring that the proposed solution is mesh independent, three additional experimental runs are reproduced numerically (Yokoi et al. [5], Patil et al. [6] and Bushan et al. [7]) and the results are compared both qualitatively as well as quantitatively.

1.3.1 Report Outline

In the present chapter (Chapter 1) an introduction to the subject of the present FYP is conducted. In more detail, a brief overview on the importance of droplet impact dynamics has been made and the main aims have been identified.

Chapter 2, contains the literature review. In more detail, in the proposed chapter a wide number of previously published works from a variety of authors and years are reviewed and the main findings and limitations are identified, in order to justify the aims of the present numerical investigation.

The overall description as well as the theoretical background (e.g. governing equations, special numerical treatments) of the adopted numerical investigation methodology are summarized in Chapter 3.

An extensive qualitative and quantitative validation of the proposed numerical model is conducted in Chapter 4, by the numerical reproduction of a series of literature available experiments of droplet impact on hydrophilic, hydrophobic and super-hydrophobic solid surfaces. The comparison of the numerical results with the corresponding experimental data indicate that the proposed enhanced VOF-based numerical model can successfully capture the spatial and temporal evolution of the droplets as these are recorded in the proposed laboratory experiments.

2.1 Literature review

In the last 20 years, many investigations of droplet impact have taken place experimentally as well as numerically. To begin, droplet impact of water on a flat, solid surface has been studied by Pasandideh-Fard et al. [3] where impacting droplets were captured by means of a high speed camera and liquid-solid contact diameters and contact angles were measured by post-processing the corresponding experimental snapshots. A numerical solution of the Navier-Stokes equations using a modified SOLA-VOF method was also used to model the interface deformation. Experimentally measured values of dynamic contact angles were used as a boundary condition for the numerical model. The impacting droplets spread on the surface until liquid surface tension and viscosity overcame inertial forces, after which they recoiled off the surface. In the experiments still water was used (0 ppm) as well as water with surfactants (100 ppm, 1000 ppm). It was observed that the addition of surfactants does not affect the shape of the droplet during the initial stages of impact, however the maximum spread diameter was increased and the recoil height was decreased. Comparing the numerical prediction with the corresponding experimental data, the simulated droplets followed the evolution of the shape of the experimental droplets correctly. The contact diameter during the spreading and at equilibrium was predicted accurately. During the recoiling stage the model over predicted the contact diameter of the droplet. The agreement of the numerical results with the experiments was improved, when the dynamic surface tension of surfactant solutions was assumed constant and equal to that of pure water. Conversely, when the contact angle was assumed constant in the model, equal to the measured equilibrium value, predictions were less accurate. Finally, capillary effects were shown to be negligible during droplet impact when We >> $Re^{\frac{1}{2}}$.

Yokoi et al. [5], investigated liquid droplet impact behavior onto a dry and flat surface, numerically. The numerical method consists of a Coupled Level Set and VOF framework (CLSVOF), a volume/surface integrated average based multi-moment method, and a continuum surface force model. Experimental results of a droplet impact have been compared with the numerical simulation predictions. It is observed that the numerical simulation reproduces the droplet behavior quantitatively, in the spreading as well as in the receding phases, only when a dynamic contact angle model was used. However, in cases where the sensible simplified dynamic contact angle model was used, the predicted time dependence of droplet behavior is poorly reproduced. Conversely, when an equilibrium angle model, as well as a static angle model was used the results were different from the experimental. Furthermore, the results using different maximum/minimum dynamic angles model, and smoothing model did not show good agreement with the experiment, either. In conclusion, in order to have precise results the dynamic contact angle modeling plays an important role in reproducing the droplet impact behavior.

Marengo et al. [8], review previous studies and investigate the hydrodynamics of a droplet impact onto a dry smooth substrate. Generally, if the Reynolds and Weber numbers are

high enough, the spreading drop can be subdivided into two main regions: a radially spreading lamella and an almost circular rim appearing due to capillary forces [9] and viscosity. In the case of drop spreading and receding, the motion of the rim is influenced also by the wall friction and by the forces associated with wettability, which depend on the dynamic contact angle [10]. The outcome of a drop impact is influenced by the impact parameters, liquid and air properties and the nature of the substrate and its topology. Several new, at the time, phenomena have been the subject of closer investigations. One phenomenon is the appearance of a very thin (of order of several nanometers) gas layer appearing at the initial stage of drop collision and deformation. The formation of this film has been recently described theoretically and numerically [10]. Another phenomenon that is related to high-speed drop impact, is the rupture of the lamella. In [11] very high impact velocities (10–30 m/s) of drops of diameters 510–650 μm have been achieved by using an experimental device with a moving target. Under these conditions the residual film thickness is comparable with the size of the microbubbles, which at some conditions leads to the expansion of holes and film rupture, the phenomenon is influenced significantly by the substrate wettability. For partially wettable surfaces the rupture threshold is determined by the Reynolds number (Re ~ 104) and the receding contact angle.

Experiments to understand the effect of surface wettability on impact characteristics of water drops onto solid dry surfaces were also conducted by Antonini et al. [9]. Many surfaces were used to cover a wide range of contact angles. In more detail, advancing contact angles from 48◦ to 166◦, and contact angle hysteresis values from 5◦ to 56◦were tested experimentally. Several different impact conditions were analyzed; 12 impact velocities on 9 different surfaces, where two of them were super-hydrophobic. Results from impact tests with millimetric drops show that two different regimes can be identified: a moderate Weber number regime (30 < We < 200), in which wettability affects both drop maximum spreading and spreading characteristic time; and a high Weber number regime (We > 200), in which wettability effect is secondary, because capillary forces are overcome by inertial effects. In particular, the results indicate the role of advancing contact angle and contact angle hysteresis as fundamental wetting parameters, to allow understanding of different phases of drop spreading and beginning of recoiling. It is also shown that drop spreading on hydrophilic and super-hydrophobic surfaces occurs with different time scales. Finally, if the surface is super-hydrophobic, eventual impalement, i.e., transition from Cassie to Wenzel wetting state, which might occur in the vicinity of the drop impact area, does not influence the drop maximum spreading.

Mitra et al. [10], investigate subcooled droplet impact on a highly thermally conductive spherical surface both theoretically and experimentally. Specifically, the effect of Weber number on spreading of droplets of three different liquids namely water, isopropyl alcohol and acetone was studied. The droplet shape evolution and surface wetting upon droplet impact at surface temperatures ranging between 20 °C and 250 °C were investigated. Maximum droplet spread was measured and compared with available correlations. Generally wetting contact was observed at surface temperatures below or close to saturation temperature whilst a non-wetting contact was exhibited at surface temperatures significantly greater than the saturation temperature. The drop in surface temperature was found to be significantly lower in this non-

wetting contact regime which led to significant reduction in heat transfer coefficient. The droplet spreading patterns in cold condition and film boiling regime were simulated using the 3D CFD models which were found to be in good agreement with the experimental observations. The droplet rebound and disintegration phenomena at lower and higher Webber numbers respectively were captured by the CFD simulations which agreed well with the high speed images from the experiments.

A three-dimensional, CLSVOF-based numerical model was developed by Gumulya et al. [11] to study the hydrodynamics of water droplets of various diameters impacting a heated solid particle. The temperature of the particle was set to be above the Leidenfrost temperature of the fluid, such that the influence of several key parameters on the dynamics of film boiling of the droplet could be examined. The simulation results were validated against experimental observations, where it was found that the numerical model could satisfactorily reproduce the dynamics of the droplet. The spread of the droplets upon impact was found to be dependent on the Weber number, with surface tension and viscous forces then acting to recoil the droplet. The rate of droplet recoil was found to be highly dependent on the Reynolds number, as fluid advection tends to enhance the rate of heat transfer within the droplet and the evaporation at the solid–liquid contact line. Eventually, evaporation causes build-up of vapour pressure at the bottom of the liquid, and the droplet lifts-off from the heated particle. It was found that the onset of the droplet lift-off could be estimated through the first-order vibration of a freely oscillating droplet, particularly in cases with low values of Weber number. Finally, the rate of evaporation of the droplet was found to be highly dependent on the capillary length of the fluid and the stability of the vapour layer formation underneath the droplet.

Microdroplets were presented by Visser et al. [12], who did both experimental and numerical simulations of microdroplet impact at velocities up to V_0= 50 m/s, on hydrophilic and hydrophobic surfaces at frame rates exceeding 107 frames per second. A novel method to determine the 3D-droplet profile at sub-micron resolution at the same frame rates is presented, using the fringe pattern observed from a bottom view. A numerical model, which is validated by the side- and bottom-view measurements, is employed to study the viscous boundary layer inside the droplet and the development of the rim. The spreading dynamics, the maximal spreading diameter, the boundary layer thickness, the rim formation, and the air bubble entrainment are compared to theory and previous experiments. In general, the impact dynamics are equal to millimeter-sized droplet impact for equal Reynolds-, Weber- and Stokes numbers (Re, We, and St, respectively). Using the numerical model simulations, effective scaling laws for the progression of the boundary layer thickness and the rim diameter are provided. The dimensionless boundary layer thickness develops in time (t) according to $\delta_{BL} \sim D_0/\sqrt{Re}\,(t/\tau)\,0.045$, and the diameter of the rim develops as DRim $\sim$ D0/ $\sqrt{We}\,(t/\tau)\,0{,}68$, with drop diameter D_0 and inertial time scale τ= D_0/V_0 . These scalings differ from previously assumed, but never validated, values. Eventually, no splash is observed, at variance with many predictions but in agreement with models including the influence of the surrounding gas. This confirms that the ambient gas properties are key ingredients for splash threshold predictions.

A novel numerical implementation for the adhesion of liquid droplets impacting normally on solid dry surfaces was presented by Malgarinos et al. [13].The benefit of this new approach, compared to the majority of existing models, is that the dynamic contact angle forming during the surface wetting process is not inserted as a boundary condition, but is derived implicitly by the induced fluid flow characteristics (interface shape) and the adhesion physics of the gas–liquid-solid interface (triple line), starting only from the advancing and receding equilibrium contact angles. The advancing and receding angles are important for defining the wetting properties of the liquid phase when interacting with a solid surface. The physical model is implemented as a source term in the momentum equation of a Navier-Stokes Computational Fluid Dynamics (CFD) flow solver as an "adhesion-like" force which acts at the triple-phase contact line as a result of capillary interactions between the liquid drop and the solid substrate. The numerical simulations capture the liquid–air interface movement by considering the volume of fluid (VOF) method and utilizing an automatic local grid refinement technique in order to increase the accuracy of the predictions at the area of interest, and simultaneously minimize numerical diffusion of the interface. Regarding the results, the model that was implemented was validated against previously experimental data on normal impingement of water droplets on dry surfaces at room temperature. A wide range of impact velocities, i.e. Weber numbers from as low as 0.2 up to 117, both for hydrophilic (θ_{adv} = 10°–70°) and hydrophobic (θ_{adv} = 105°–120°) surfaces, has been examined. Predictions include in addition to droplet spreading dynamics, the estimation of the dynamic contact angle; the latter is found in reasonable agreement against available experimental measurements. It is thus concluded that the implementation of this model is an effective approach for overcoming the need of a pre-defined dynamic contact angle law, frequently adopted as an approximate boundary condition for such simulations. Clearly, this model is mostly influential during the spreading phase for the cases of low We number impacts (We < ~80) since for high impact velocities, inertia dominates significantly over capillary forces in the initial phase of spreading.

Zhang et al. [14] investigated the phenomenon of spray impinging on in-cylinder walls. This phenomenon has important impact on combustion processes as well as harmful emissions for internal combustion engines. It is known that spray/wall impinging process is affected by the physical properties of the droplet, the motion status of the surrounding air and the surface condition of the walls. The method of VOF and liquid-solid wetting model are adopted to carry out numerical simulation of the impinging processes between spray micro-droplets and walls. The results show that the droplet scale has important effect on the impinging process. It has been found that for the big droplet experiments the critical number for splash/non-splash boundary, may not suitable for spray micro-droplets in engine application. Taking into account that, the influence of a variety of factors on the micro-droplets/wall impinging process is researched. The results show that, compared to big droplets, the physical properties of liquid more strongly affect the micro-droplet spreading process and the dynamic viscosity coefficient has greater impact than the surface tension. Also it was found that the surface tension of liquid only has a little influence on the splashed liquid mass and the wall film spreading process, the dynamic viscosity

significantly affects the amount of splash and the spreading radius and thickness of the wall film after impinging. The presence of a thin film on the wall will promote splashes. The critical parameter K to determine the droplet splash/non-splash boundary changes from $K = Re^{1/4} \times We^{1/2}$ (for millimeter diameter droplet) to $K = Re^{1/2} \times We^{1/3}$ (for spraymicro-droplet).

Droplet impact with a numerical methodology for modeling contact line motion in a dual – grid level – set method (DGLSM) on hydrophobic and superhydrophobic surfaces was implemented by Patil et al. [6]. Particularly, a quasi - dynamic contact angle model – based on experimental inputs – is implemented to model the dynamic wetting of a droplet, impacting on a hydrophobic or a superhydrophobic surface. Non bouncing and bouncing experiments on hydrophobic surfaces are presented on this paper. The DGLSM based numerical results are in aggrement with the experimental results of the droplet impact (both for the diameter and the height of the droplet). Experimental results that have already been published for non-bouncing on hydrophobic and bouncing on superhydrophobic surface, at constant velocity, are also compared with numerical results in this paper. Furthermore, qualitative as well as quantitative performance of the DGLSM as compared to the traditional level set method (LSM) is presented by considering the same experimental results. The accuracy of the partially refined DGLSM is close to that of the fine – grid based LSM, at a computation cost which is close to that of the coarse – grid based LSM. The DGLSM is demonstrated as an improved LSM for the computational multi-fluid dynamics simulations involving contact line motion.

3.1 Numerical Methodology

3.1.1 Governing equations

In general, with the VOF approach, the transport equation for the volume fraction, α, of the secondary (dispearsed) phase is solved simultaneously with a single set of continuity and Navier–Stokes equations for the whole flow field [15]. The corresponding volume fraction of the primary phase is simply calculated as (1-α). The main underlying assumptions are that the two fluids are Newtonian, incompressible, and immiscible. The governing equations can be written as:

$$\nabla \times \vec{U} = 0 \tag{1}$$

$$\frac{\partial \rho_b}{\partial t} + \nabla \times \left(\rho_b \vec{U} \vec{U} \right) = -\nabla_p + \nabla \times \mu_b \left(\nabla \vec{U} + \nabla U^T \right) + \rho_b f + F_s \tag{2}$$

$$\frac{\partial a}{\partial t} + \nabla \times \left(a\vec{U} \right) = 0 \tag{3}$$

where U is the fluid velocity, p the pressure, f the gravitational force, and Fs the volumetric representation of the surface tension force. The bulk density ρ_b and viscosity μ_b are computed as the averages over the two phases, weighted with the volume fraction α:

$$\rho_b = \rho\alpha + \hat{\rho}\,(1-\alpha) \tag{4}$$

$$\mu_b = \mu\alpha + \hat{\mu}\,(1-\alpha) \tag{5}$$

where ρ, $\hat{\rho}$, μ and,$\hat{\mu}$ are the densities and the viscosities of the two phases. In the VOF method, α is advected by the fluids. For the case of incompressible flow, this is equivalent to volume fraction conservation, which makes the method mass conservative.

The surface tension force is modelled as a volumetric force using the Continuum Surface Force (CSF) method by Brackbill et al. [16] applying the following equations:

$$F_s = \gamma\kappa\,(\nabla\alpha) \tag{6}$$

$$\kappa = \nabla\left(\frac{\nabla\alpha}{|\nabla\alpha|}\right) \tag{7}$$

where γ is the tension of the interface and κ is the curvature of the interface.

3.2.1 Sharpening of the interface:

Interface sharpening is very important in simulating two-phase flows of two immiscible fluids. In OpenFOAM the sharpening of the interface is achieved artificially by introducing an extra compression term in the advection equation of α. Therefore, equation (3) in OpenFOAM is modified and transformed to the following equation:

$$\frac{\partial a}{\partial t} + \nabla \times \left(a\vec{U}\right) - \nabla \times (a\,(1-a)U_r = 0 \tag{8}$$

U_r is the artificial compression velocity with is calculated from the following relationship :

$$U_r = n_f \min\left[C_\gamma \frac{|\phi|}{|S_f|}, \max\left(\frac{|\phi|}{|S_f|}\right)\right] \tag{9}$$

where n_f is the cell surface normal vector, ϕ is the mass flux, $S_f$is the surface area of the cell, and C_γ is a coefficient, the value of which can be set between 0 and 4. U_r is the relative velocity between the two fluids due to the density and viscosity change across the interface. In equation (9) the divergence of the compression velocity U_r, ensures the conservation of the volume fraction α, while the term α (1-α) limits this artificial compression approach only in the vicinity of the interface, where 0 <α< 1 [17]. The level of compression depends on the value of C_γ[17,18]. For the simulations of the present investigation, initial, trial simulations indicated that a value of C_γ=1 should be used, in order to maintain a quite sharp interface without at the same time having unphysical results.

3.3.1 VOF smoothing:

The VOF method usually suffers from non-physical spurious currents in the interface region. These spurious velocities are due to errors in the calculation of the normal vectors and the curvature of the interface that are used for the calculation of the interfacial forces. These errors emerge from the fact that in the VOF method the interface is implicitly represented by the volume fraction values that encounter sharp changes over a thin region. In the present investigation, an improved VOF method where the spurious currents are suppressed by appropriate modifications of the original VOF-based solver of OpenFOAM (interFoam), is utilized [15]. The proposed modification involves the calculation of the interface curvature κ using the smoothed volume fraction values $\tilde{\alpha}$, that are obtained from the initially calculated α field, smoothing it over a finite region in the vicinity of the interface. All other equations are using the initially calculated (non-smoothed) volume fraction values of α. Therefore, instead of equation (8) the following equation is used for the interface curvature calculation [15]:

$$\kappa = \nabla \cdot \left(\frac{\nabla \tilde{\alpha}}{|\nabla \tilde{\alpha}|} \right) \tag{10}$$

The proposed smoothing is achieved by the application of a Laplacian filter which can be described by the following equation [15]:

$$\tilde{a}_p = \frac{\sum_{f=1}^{n} a_f S_f}{\sum_{f=1}^{n} S_f} \tag{11}$$

In Equation (11), the subscripts p and f denote the cell and face index respectively and a_f is the linearly interpolated value of α at the face center. The application of the proposed filter can be repeated more than one times in order to obtain an adequately smoothed field. In the applications of the present investigation, the filter is applied 2 times in order to avoid the leveling out of high curvature regions.

3.4.1 Simulation parameters:

All the numerical simulations that will be presented in the current FYP were performed with the finite-volume-based CFD code OpenFOAM (version 2.2.1). For pressure–velocity coupling, the PISO (pressure-implicit with splitting of operators) scheme is applied. The transient terms in the equations are discretized using a second order, bounded, implicit scheme (Crank Nicolson). The calculation time step is controlled by setting the maximum Courant number to 0.2. With this adaptive time step technique, the time step was automatically varied from approximately 10^{-8} to 10^{-6} sec. The gradient terms are discretized using a second order, Gaussian integration with linear interpolation (Gauss linear). For the divergence terms different discretization schemes are applied for each term in the equations. In more detail the convection term of equation (2) is discretized using a Gauss limited linear scheme in order to produce good accuracy, with the value of the required coefficient ϕ equal to unity, since this value ensured better stability during the calculations (Gauss limitedLinearV 1.0). The $\nabla \cdot \left(\alpha \vec{U}\right)$ term of equation (8) is discretised using the "Gauss vanLeer" scheme, while the $\nabla \cdot \left(a(1-a)U_r\right)$ term is discretised using the "Gauss interface Compression" scheme that ensures the boundedness of the calculated volume fraction field. Finally, all laplacian terms are discretized using the "Gauss Linear Corrected" scheme. Further details regarding the adopted discretization schemes can be found in OpenFOAM Documentation [19].

3.5.1 Contact angle treatments:

Criscione [20] et al. (presented a work where they explain the implementation of three different schemes that can be implemented regarding the contact angle between the droplet and the impact surface. In more detail, the spreading and receding behavior of simulated water droplets impacting onto automobile wind shields or aircraft wings is not only determined by their initial conditions, but also influenced by the evolution of the contact angle throughout the specific in each case impact scenario. Hence, a physically correct representation of the dynamic contact angle is desired to obtain useful results when performing multiphase simulations of impacting drops. Several models predict the evolution of the fluid's contact angle. One approach for predicting the evolution of the fluid's contact angle is to assign a constant value to the equilibrium contact angle, thus neglecting the contact angle hysteresis. This is also referred to as a static contact angle model. Using a constant contact angle, under the following assumption,

$We_0 \gg 1$, yields quite accurate results for the spreading phase of the drop impact where the lamella flow is inertia dominated, but however not for the receding phase [21]. An alternative way to model the contact angle is to apply a varying contact angle, which depends on instantaneous flow parameters. These models are called dynamic contact angle models. OpenFOAM® already comes with an implemented dynamic contact angle model that is applied by selecting "dynamicAlphaContactAngle" as boundary condition for the volume of fluid function at walls. Apart from the pre-implemented dynamic model, the user can also specify constant contact angles by either choosing a zeroGradient boundary condition to represent an angle of $\theta_0 = \theta_A = \theta_R = 90°$ or by selecting the constantAlphaContactAngle boundary condition for arbitrary constant angles.

In this work, three different approaches of contact angles (Static, Dynamic, and Kistler Dynamic Contact Angle) were implemented and compared with the experimental results presents in the works of Pasandideh et al. [4] as well as Yokoi et al. [5], Patil et al [6] and Bushan et al. [7]

3.5.2 Static (Constant) Contact Angle:

When a static contact angle treatment is utilized, at the solid/wall boundaries of the computational domain, an equilibrium contact angle is imposed as θe. The contact angle θe is used in order to calculate the surface normal ($\vec{n}$) in the adjacent to the wall boundaries computational cells, where the two fluid phases are in direct contact with the solid surface, utilizing the following relationship:

$$\vec{n} = \vec{n}_n \cos\theta_e + \vec{n}_t \cos\theta_e \qquad (12)$$

where $\vec{n}_n$ and $\vec{n}_t$ are the unit vectors at the directions normal and tangential to the solid wall, respectively [15]

3.5.3 Dynamic Contact Angle:

Many suggestions regarding Dynamic CA have been given. Saha et al. [22], Jiang et al. [23] suggested empirically that the dependence of the dynamic contact angle on the contact line velocity is given by,

$$cos\theta_d = \cos\theta_\varepsilon - (1 + \cos\theta_\varepsilon)\tanh(4.96\, C_a^{0.702}) \quad (13)$$

A dependence of the dynamic contact angle on the contact line velocity is suggested by Shikhmurzaev [24], and is given as

$$cos\theta_d = \cos\theta_\varepsilon - \frac{2u(a_1 + a_2\, u_0)}{(1-a_2)[(a_1 + u^2)^{0.5} + u} \quad (14)$$

where $u = a_3\, \frac{\mu v}{\sigma}$, $u_0 = \frac{sin\theta_d - \theta_d \cos\theta_d}{sin\theta_d\, \cos\theta_d - \theta_d}$, a_1 = 1+ (1- a_2) (cos θ_ε − a_4) and a_2 , a_3 and a_4 are some phenomenological constants (0.54, 12.5 and 0.07 respectively).

However, the Dynamic CA model which was implemented in OpenFOAM for our numerical work is suggested by,

$$\text{Constant} \times\ C_a = \theta^3_{dynam.} - \theta^3_{equil.} \quad (15)$$

where

$$C_a = \frac{\mu \times V}{\sigma},$$

with μ - dynamic viscosity, V - velocity of the contact line, and σ (sigma) - surface tension, θ – contact angle (rad). Constant is found from fitting this expression to the experimental data for a given range of the from velocities. The expression works well for Ca<1 (typically up to Ca = 0.1).

3.5.4 Kistler Dynamic Contact Angle:

One of the most recent and accurate contact angle models is the Kistler model [25], which calculates the dynamic contact angle, Θ_{dyn}, using the Hoffman function, f_{Hoff} , as follows:

$$\Theta_{dyn} = f_{Hoff} [C_a + f_{Hoff}^{-1} (\Theta_e)], \qquad (16)$$

where Θ_e is the equilibrium contact angle. The capillary number, C_a , is built according to $C_a = U_{cl} \frac{\mu}{\sigma}$, where U_{cl}, μ and σ are the spreading velocity of the contact line, the dynamic viscosity of the liquid and the surface tension of liquid and gas phase, respectively. The f_H^{-1} is the inverse function of the "Hoffman's" empirical function which is given in the following form [Criscione et al. 26].

$$f_H = acros \{ 1 - 2 \tanh [5.16 [\frac{\chi}{1+1,31\ \chi^{0,99}}]^{0.706}] \} \quad (17)$$

Equation (16) shows that Θ_{dyn} depends significantly on the capillary number of the contact line and requires the input of an equilibrium contact angle. For surface s which are not ideally smooth, i.e. which show a distinct contact angle hysteresis, the equilibrium angle Θ_e is replaced by either a limiting advancing or receding contact angle Θ_{Adv} or Θ_{Rec} , respectively, depending on the sign of the velocity vector at the contact line. Note that $\Theta_{Adv}$and Θ_{Rec} are system properties that are determined from experiments by Roisman et al. [27].

3.6.1 CFD software information

OpenFOAM®

For our numerical work we used OpenFOAM® 2.2.1 installed in Linux Ubuntu 13.04. OpenFOAM is a free, world leading, open source Computational Fluid Dynamics [CFD] software package developed by OpenCFD Ltd, in 2004 at ESI Group and distributed by the OpenFOAM Foundation. It is used for various engineering and science aspects such as, chemical reactions, turbulence and heat transfer, to solid dynamics, acoustics and electromagnetics.

The basic directory structure for a OpenFOAM® case, that contains the minimum of 3 set of folders required to run an application. These folders namely are: 0 (zero) folder, constant folder and system folder. Turning to the detail, the 0 folder, can be: either, initial values and boundary conditions that the user must specify to define the problem; or, results written to folder by OpenFOAM. Our 0 folder contains the initial conditions of our droplet at time t = 0, such us velocity U, pressure P, and also a file called alpha 1 (Figure 1) in which we indicate the contact angle model as well as, the contact angles (Equilibrium CA, Advancing CA and Receding CA).

```
/*--------------------------------*- C++ -*----------------------------------*\
| =========                 |                                                 |
| \\      /  F ield         | OpenFOAM: The Open Source CFD Toolbox           |
| \\    /   O peration      | Version:  1.5.x                                 |
| \\  /    A nd             | Web:      http://www.OpenFOAM.org               |
|  \\/     M anipulation    |                                                 |
\*---------------------------------------------------------------------------*/
FoamFile
{
    version     2.0;
    format      ascii;
    class       volScalarField;
    location    "0";
    object      alpha1;
}
// * * * * * * * * * * * * * * * * * * * * * * * * * * * * * * * * * * * * //

dimensions      [0 0 0 0 0 0 0];

internalField  uniform 0;

boundaryField
{
    top
    {
        type            zeroGradient;
        value           uniform 0;
    }
    bottom
    {
        type dynamicAlphaContactAngle;
value uniform 1;
theta0 90;
uTheta 1;
thetaA 110;
thetaR 40;
```

Figure 1: alpha1 directory which is contained in 0 folder

The constant directory that contains a full description of the case mesh in a subdirectory polyMesh and files specifying physical properties for the application concerned, e.g. transportProperties, gravity and blockMeshDIct. In the blockMeshDict (Fugure 2) we define the geometry of our computational domain which in our cases is hexahedral. Also we define the cells of our computational domain. Particularly in our cases the cells will be 1000 (x Axis) x 1600 (y Axis) x 1 (z Axis), this means that n total our simulation is 1.6 million cells.

```
/*--------------------------------*- C++ -*----------------------------------*\
| =========                 |                                                 |
| \\      / F ield          | OpenFOAM: The Open Source CFD Toolbox           |
| \\    / O peration        | Version:  1.5                                   |
| \\  /   A nd              | Web:      http://www.OpenFOAM.org               |
|  \\/    M anipulation     |                                                 |
\*---------------------------------------------------------------------------*/
FoamFile
{
    version    2.0;
    format     ascii;
    class      dictionary;
    object     blockMeshDict;
}
// * * * * * * * * * * * * * * * * * * * * * * * * * * * * * * * * * * * * //

convertToMeters 1.0e-3;

vertices
(
    (0 0 -0.2181e-3)//0
    (5 0 -0.2181)//1
    (5 8 -0.2181)//2
    (0 8 -0.2181e-3)//3
    (0 0 0.2181e-3)//4
    (5 0 0.2181)//5
    (5 8 0.2181)//6
    (0 8 0.2181e-3)//7
);

blocks
(
    hex (0 1 2 3 4 5 6 7) (1000 1600 1) simpleGrading (5 5 1)
);
```

Figure 2: blockMeshDict file

```
/*--------------------------------*- C++ -*----------------------------------*\
| =========                 |                                                 |
| \\      / F ield          | OpenFOAM: The Open Source CFD Toolbox           |
| \\    / O peration        | Version:  2.2.1                                 |
| \\  /   A nd              | Web:      www.OpenFOAM.org                      |
|  \\/    M anipulation     |                                                 |
\*---------------------------------------------------------------------------*/
FoamFile
{
    version    2.0;
    format     ascii;
    class      dictionary;
    location   "constant";
    object     transportProperties;
}
// * * * * * * * * * * * * * * * * * * * * * * * * * * * * * * * * * * * * //

phase1
{
    transportModel  Newtonian;
    nu              nu [ 0 2 -1 0 0 0 0 ] 1e-06;
    rho             rho [ 1 -3 0 0 0 0 0 ] 1000;
    CrossPowerLawCoeffs
    {
        nu0         nu0 [ 0 2 -1 0 0 0 0 ] 1e-06;
        nuInf       nuInf [ 0 2 -1 0 0 0 0 ] 1e-06;
        m           m [ 0 0 1 0 0 0 0 ] 1;
        n           n [ 0 0 0 0 0 0 0 ] 0;
    }

phase2
{
    transportModel  Newtonian;
    nu              nu [ 0 2 -1 0 0 0 0 ] 1.48e-05;
    rho             rho [ 1 -3 0 0 0 0 0 ] 1;
    CrossPowerLawCoeffs
    {
        nu0         nu0 [ 0 2 -1 0 0 0 0 ] 1e-06;
        nuInf       nuInf [ 0 2 -1 0 0 0 0 ] 1e-06;
        m           m [ 0 0 1 0 0 0 0 ] 1;
        n           n [ 0 0 0 0 0 0 0 ] 0;
    }

sigma           sigma [ 1 0 -2 0 0 0 0 ] 0.07;
```

Figure 3: transportProperties file

In the transportProperties (Figure 3) file we define the properties of our droplet (phase 1), such us the kinematic viscosity nu and the density ρ, as well as the properties of the air (phase 2). Moreover, we define the surface tension σ.

Last but not least, is the system directory [b], in which contains at least the following 3 files: controlDict (Figure 4) where run control parameters are set including start/end time, time step and parameters for data output; fvSchemes where discretization schemes used in the solution may be selected at run-time; and, fvSolution where the equation solvers, tolerances and other algorithm controls are set for the run. In addition, our folder containts directories such us decomposePartDict where we define the number of the cores, which depends on the number of cells. In our cases we used 12 cores (3 4 1) in x , y and z axis respectively. Apart from the decomposePartDict, we have another file called, setFieldsDict (Figure 5). In the setFieldsDict we define parameters such as the velocity of the droplet, the direction of the droplet and the dimensions of the droplet (the radius from the 0 point of the x and y of our computational domain).

```
/*--------------------------------*- C++ -*----------------------------------*\
| =========                 |                                                 |
| \\      / F ield          | OpenFOAM: The Open Source CFD Toolbox           |
| \\    / O peration        | Version:  2.2.1                                 |
| \\  /   A nd              | Web:      www.OpenFOAM.org                      |
|  \\/    M anipulation     |                                                 |
\*---------------------------------------------------------------------------*/
FoamFile
{
    version     2.0;
    format      ascii;
    class       dictionary;
    object      setFieldsDict;
}
// * * * * * * * * * * * * * * * * * * * * * * * * * * * * * * * * * * * * //

defaultFieldValues
(
    volScalarFieldValue alpha1 0
    volVectorFieldValue U (0 0 0)
);

regions
(

sphereToCell
    {
        centre (0 1.000e-3 0);
        radius 1.000e-3;
        fieldValues
        (

            volScalarFieldValue alpha1 1
            volVectorFieldValue U (0 -1 0)

        );
    }
```

Figure 5: setFieldsDict file

```
/*--------------------------------*- C++ -*----------------------------------*\
| =========                 |                                                 |
| \\      / F ield          | OpenFOAM: The Open Source CFD Toolbox           |
| \\    / O peration        | Version:  2.2.0                                 |
| \\  /   A nd              | Web:      www.OpenFOAM.org                      |
|  \\/    M anipulation     |                                                 |
\*---------------------------------------------------------------------------*/
FoamFile
{
    version     2.0;
    format      ascii;
    class       dictionary;
    location    "system";
    object      controlDict;
}
// * * * * * * * * * * * * * * * * * * * * * * * * * * * * * * * * * * * * //

application     myInterFoamVOFSmooth;

startFrom       latestTime;

startTime       0;

stopAt          endTime;

endTime         0.0105;

deltaT          0.000001;

writeControl    adjustableRunTime;

writeInterval   0.00005;

purgeWrite      0;

writeFormat     ascii;
```

Figure 4: controlDict file

4.1 Validation of Numerical Model

4.1.1. *Computational domain and boundary conditions:*

First of all, in order to plan out our simulation it is important to define our geometry. Apart from the dimensions of the droplet, the computational domain of the droplet has to be implemented. This has already been defined in the constant file and particularly in the blockMeshDict. As you can see in the Figure 6, the computational domain for all of the numerical work (cases) of this dissertation will have the same dimensions, 5 mm width and 8 mm length. This is due to respect of the minimum domain dimensions according to OpenFOAM user guide [28], which depends from our droplet diameter.

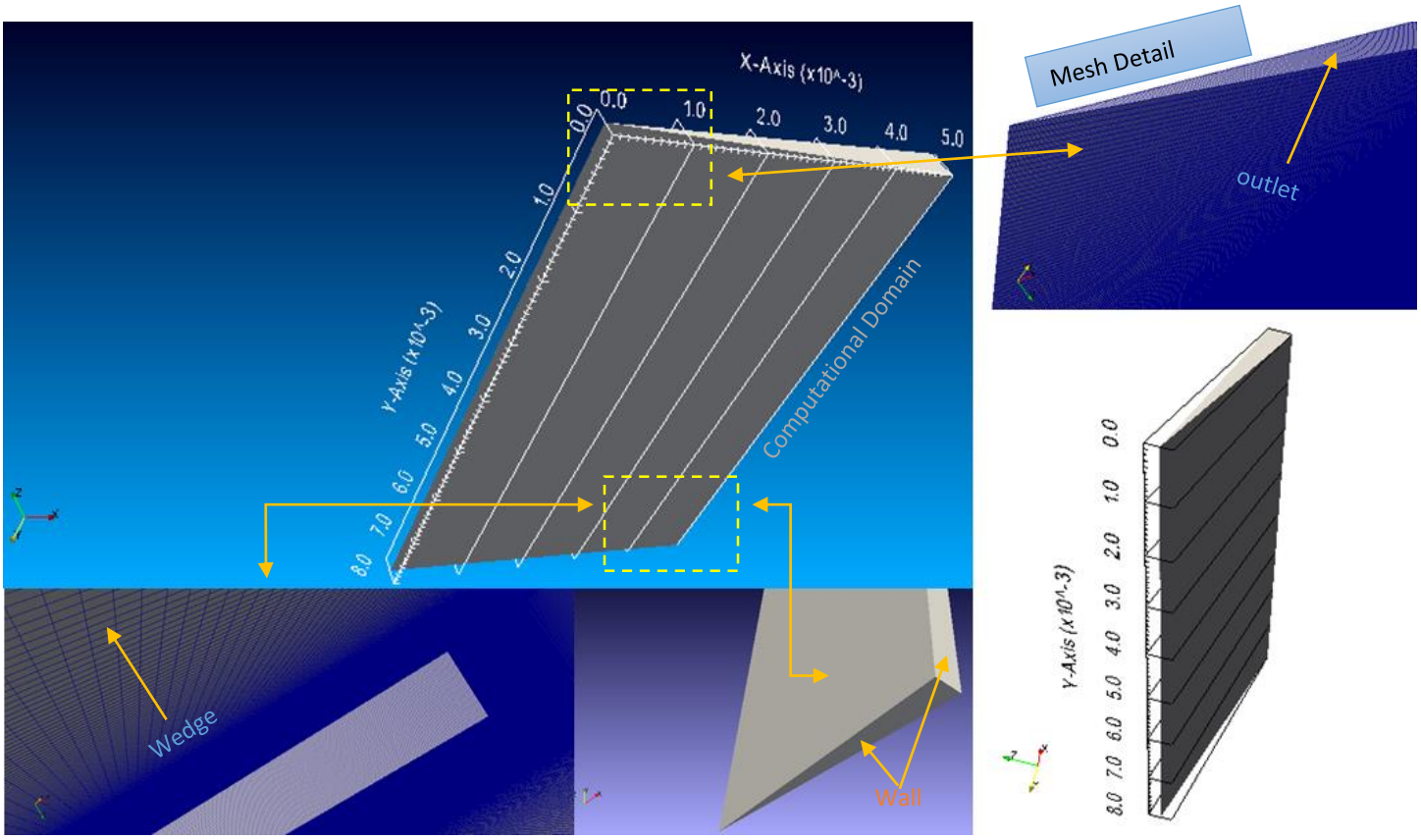

Figure 6: Different angles of Computational domain, mesh and boundary conditions with respect of the dimensions of the droplet

4.2 Problem definition

4.2.1 *Experiment I*

In order to validate our numerical model, comparisons with three different experiments have been made. The first experiment is by Pasandideh et al. [4]. Single droplets were formed by forcing water from a syringe pump through a hypodermic needle and letting them detach under their own weight. Droplets fell onto a polished stainless steel surface placed 50 mm below the needle tip. Their impact velocity, 1 m/s, was low enough that droplets did not shatter upon impact. By varying the time delay between the droplet first touching the surface and triggering of the flash, different stages of droplet impact could be photographed. Droplet release and impact were sufficiently repeatable that the entire droplet deformation process could be reconstructed from photographs of different droplets, captured at progressively advancing stages of impact. The experiment was verified the repeatability of our measurements by photographing five different droplets at the same instant after impact. This was repeated for ten different time delays. Measurements of the contact angle were reproducible within $\pm 2°$, and of contact diameter within ± 0.1 mm, on a hydrophobic surface. The droplet is pure water with diameter 2.05$\pm$ 0.03 mm, density ρ 1000 $\frac{m^3}{kg}$, dynamic viscosity μ (mu) 9.98 $\times$ 10^{-4} $\frac{kg}{\sec m}$, surface tension γ or σ 73 $\frac{mNt}{m}$, Webber (We = $\frac{\rho V_0 D_0^2}{\gamma}$) and Reynolds (Re = $\frac{V_0 D_0}{\upsilon}$) number are 27 and 2112 respectively. The same dimensions and properties were used as parameters in our numerical simulations.
Regarding contact angles, the equilibrium contact angle was measured θ_{eq} = 90°.

The following pictures show the experimental results of droplet impact of pure water in different time periods by Pasandideh et a. [4]

Figure 7: 8 different time periods of droplet impacting a stainless steel surface with a velocity of 1 m/s from Pasandideh's et al. experiment [4]

4.2.2 *Numerical results with respect of Experiment I*

Static contact angle, dynamic contact angle and dynamic Kistler contact angle models have been applied in order to reproduce numerically the experiment by Pasandideh et al. [3]. We named constant contact angle's data, Case 1, the dynamic contact angle Case 2, and the dynamic Kistler contact angle Case 3. All the numerical simulations consist of 1.6 million cells.

4.2.3 Case 1

In this case it is used the constantAlphaContactAngle model in the alpha1 file. The angle that was used is that contact angle $\theta_{advancing} = 110°$.

The following figures are the numerical results of Case 1 (right side), compared with the corresponding experimental snapshots [3]:

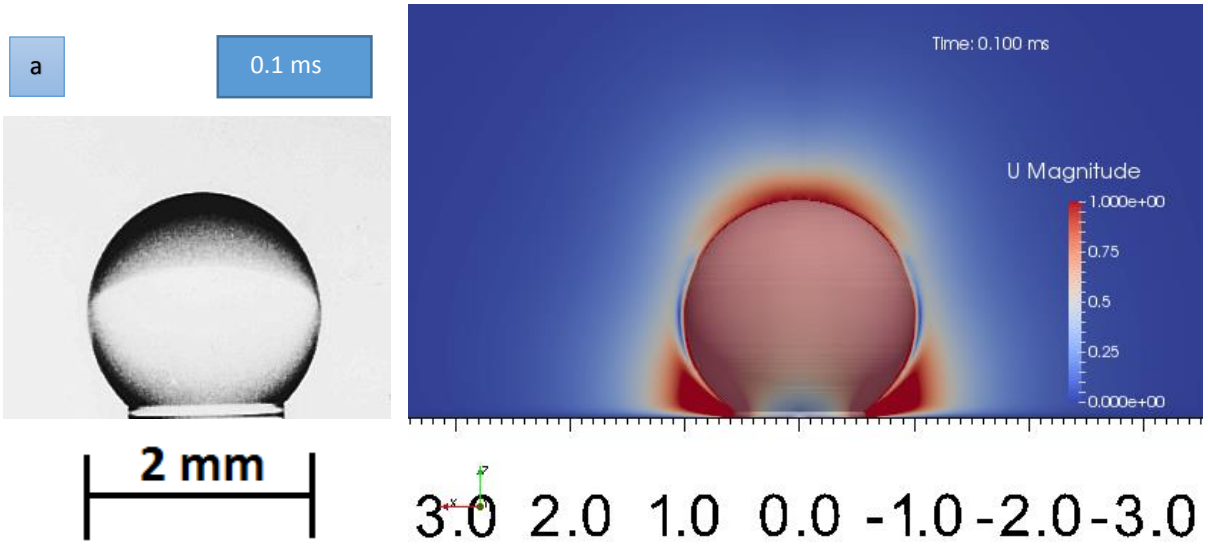

b

0.3 ms

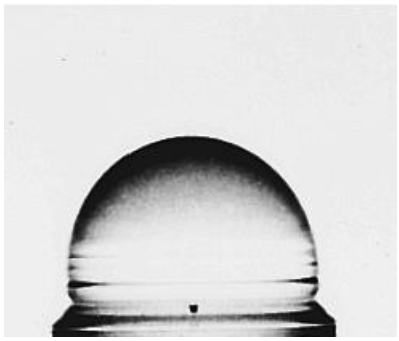

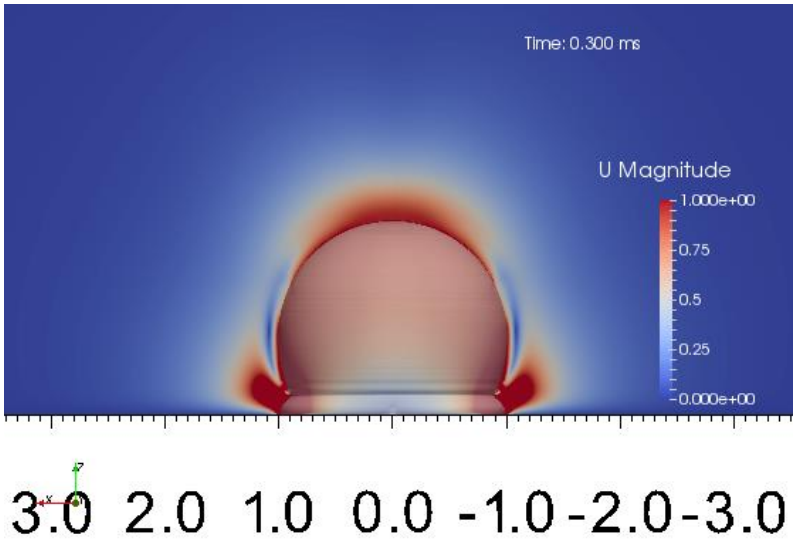

2 mm

3.0 2.0 1.0 0.0 -1.0 -2.0 -3.0

c

1.3 ms

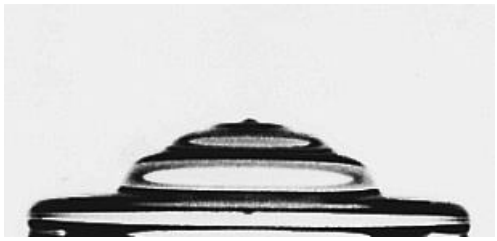

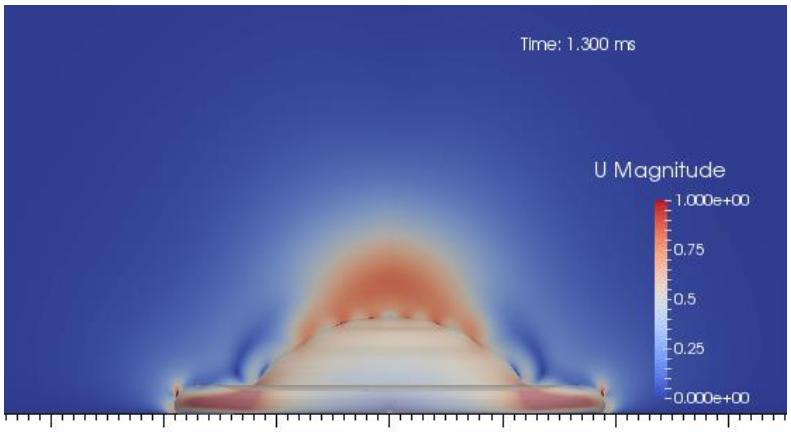

2 mm

3.0 2.0 1.0 0.0 -1.0 -2.0 -3.0

d

2.6 ms

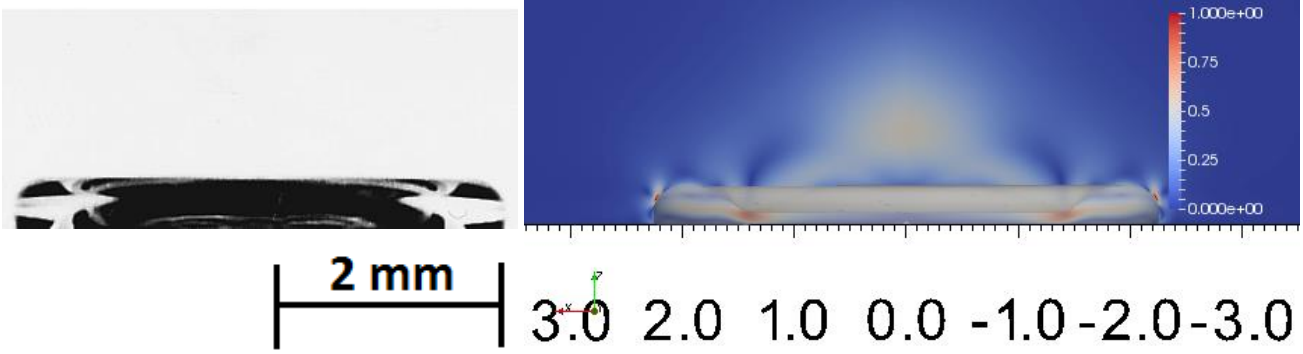
Time: 2.600 ms
U Magnitude
1.000e+00
0.75
0.5
0.25
0.000e+00

2 mm
3.0 2.0 1.0 0.0 -1.0 -2.0 -3.0

e

6.2 ms

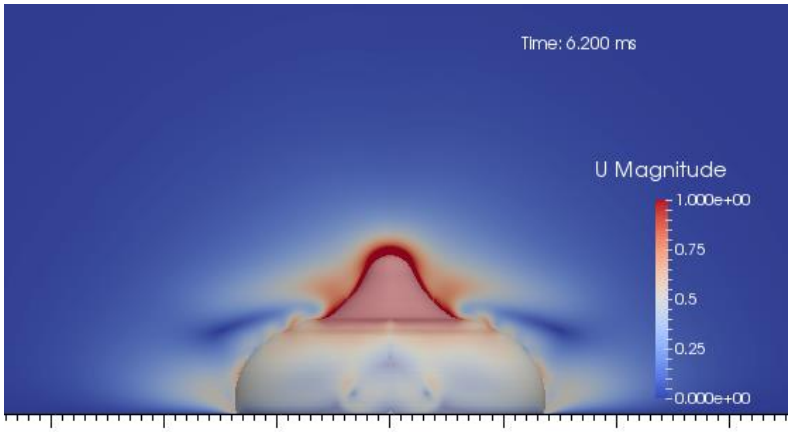
Time: 6.200 ms
U Magnitude
1.000e+00
0.75
0.5
0.25
0.000e+00

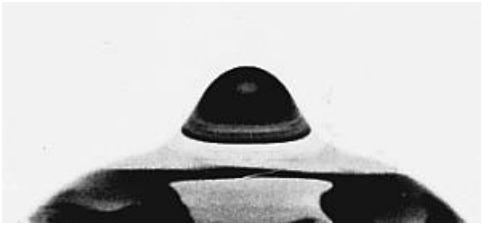


2 mm
3.0 2.0 1.0 0.0 -1.0 -2.0 -3.0

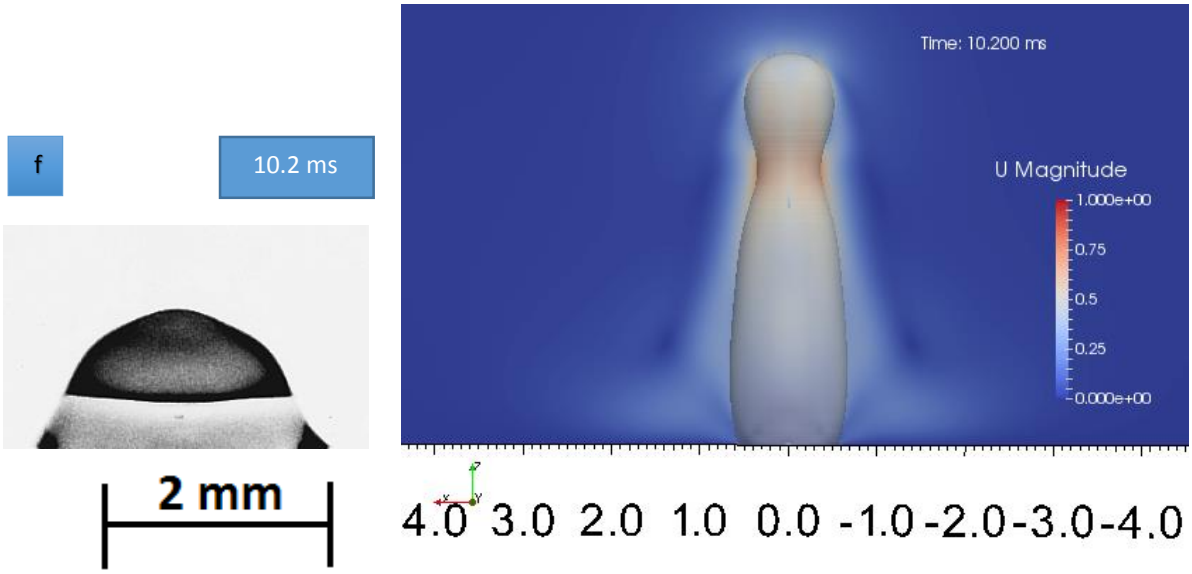

Figure 8: (a,b,c,d,e,f) Spatial and temporal evolution of droplet after the time of impact. Numerical (right) and experimental (left) snapshots.

The above figures are results of constant contact angle model, with 1.6 million cells. The background blue to red coloring represents the velocity magnitude. The most redish the color the closer to 1 m/s which is the value of the droplet velocity at the time of impact.

As we can see, comparisons have been made for 6 different time periods 0.1 ms, 0.3 ms, 1.3 ms, 2.6 ms, 6.2 ms and 10.2 ms. For the time periods 0.1 ms , 0.3 m, 1.3 ms and 2.6 ms the numerical results shows good agreement with the experimental results by Pasandideh et al, however there is some difference in the maximum spreading diameter of the droplet between numerical end experimental results (more details in the total comparison diagram, in Table 1 and Graph 1). Conversely, the time period 6.2 ms and 10.2 ms of the numerical results of constant contact angle do not show good agreement with the experimental. This is due to fact that a constant contact angle boundary condition is used in this case with the same value as the advancing CA determined from the experiments. However, in reality the contact angle is dynamic and it varies between 2 extreme values of advancing and receding angles that correspond to the 2 major stages of the droplet (spreading and recoling).

4.2.4 Case 2

In this case we will use dynamicAlphaContactAngle as boundary condition for the volume of fluid function at walls. This model has the advantage of defining more options regarding to contact angles (advancing and receding), the the constant CA model. As it is indicated in Figure 1, the equilibrium CA has value 90°, the advancing and receding CA are 110° and 40° respectively.

- Comparison of numerical results of Case 2 with the results of Experiment I:

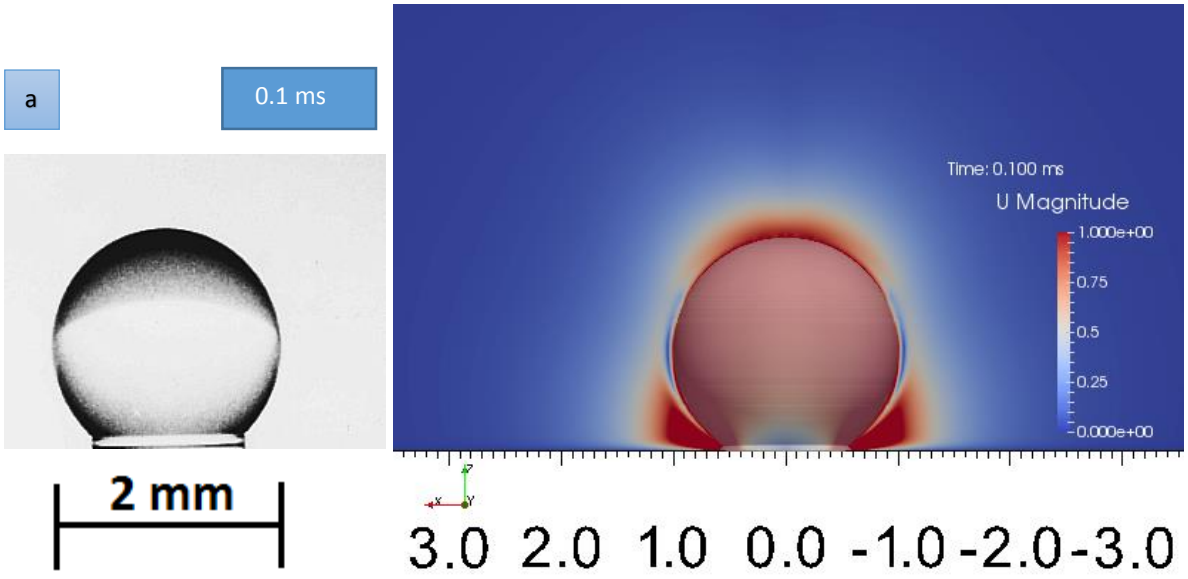

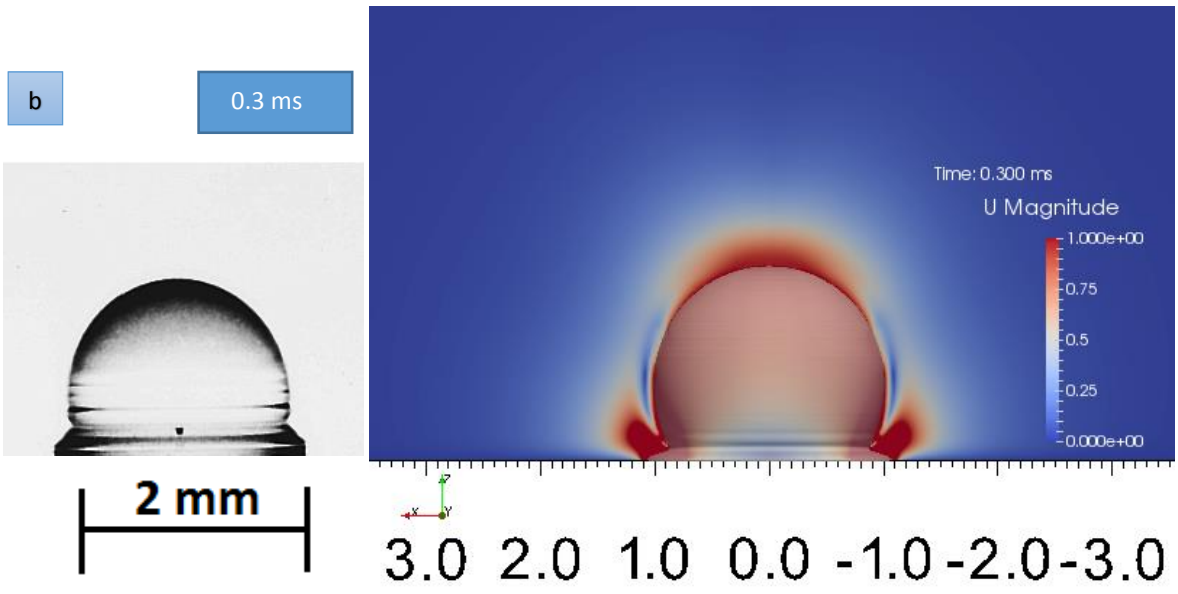

c

1.3 ms

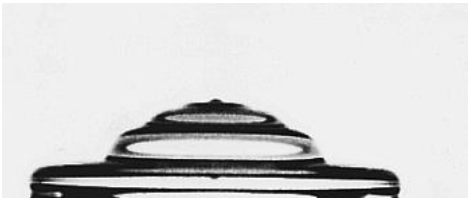

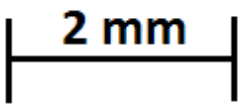

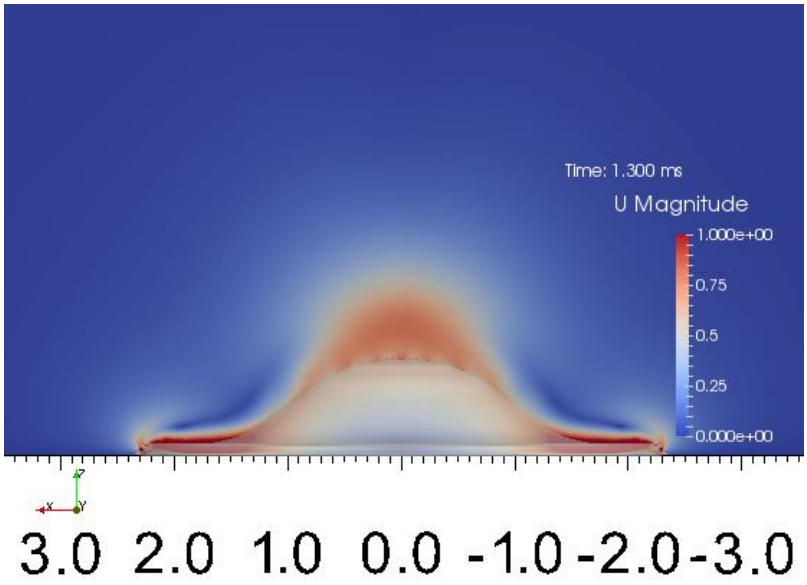

d

2.6 ms

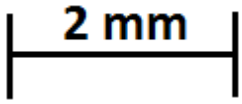

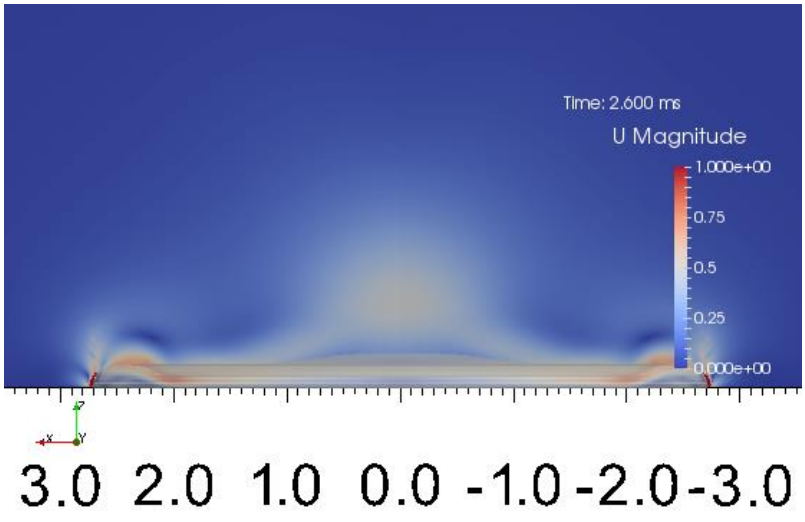

e

6.2 ms

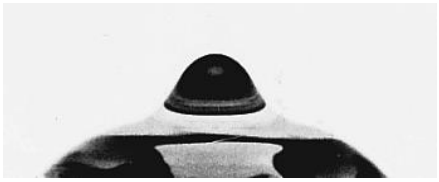

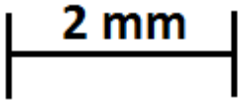

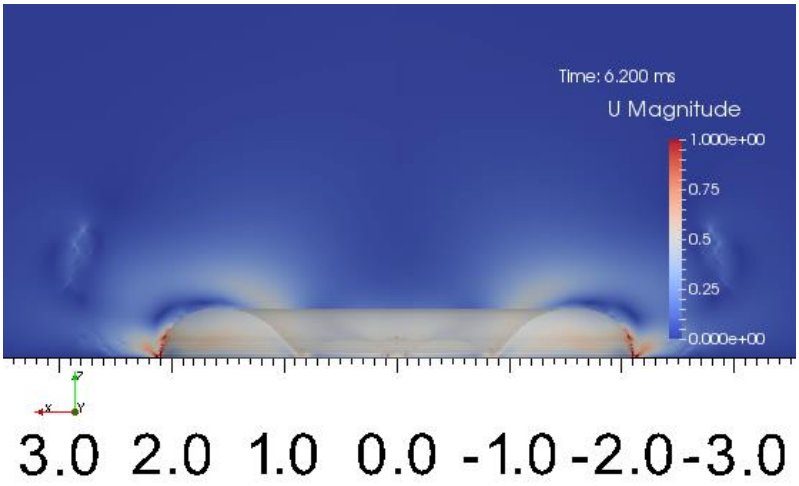

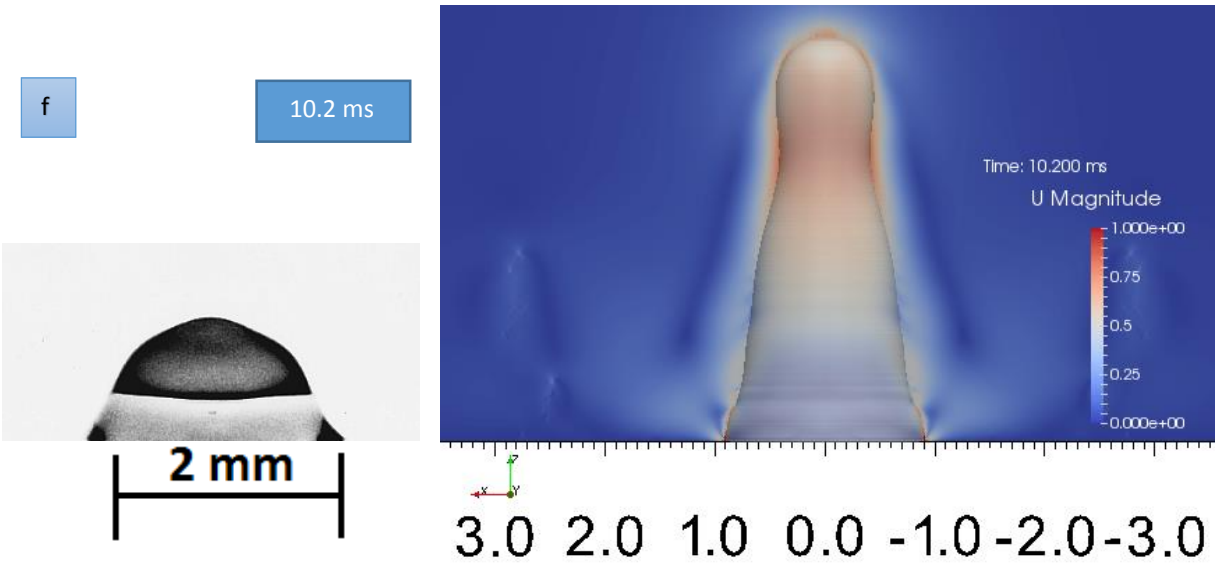

Figure 9: (a,b,c,d,e,f) Spatial and temporal evolution of droplet after the time of impact. Numerical (right) and experimental (left) snapshots.

Case 2 shows even worse results comparing to experimental ones, than Case 1. In more detail, time steps of up to 0.1 ms, 0.3 ms, predicted well the spreading of the droplet, however in the next time steps the Dynamic CA model do not show good agreement with the experimental results. In time period 6.2 ms the numerical simulation shows a small delay and the maximum diameter is bigger than the experiment, hence the results are not accurate. In the time period of 10.2 ms the recoil of the droplet in the numerical simulation is faster and do not show good agreement with the experimental results, however the maximum diameter of Case 2 (1.8mm) in the time period 10.2ms is closer to experimental (2.50mm), comparing to Case 1 (1.1mm). Overall, comparing to Case 1, Case 2 shows less accurate results.

4.2.5 Case 3

In this case we are using the dynamicKistlerAlphaContactAngle model. Comparing to Dynamic CA model of Case 2, the Kistler model is expected to be even more accurate according to literature [22] [24], this is due to the fact that the Kistler model does not rely on empirical parameters (scaling velocity) as the Dynamic CA model does. The values of contact angles that are specified in the proposed model are, maximum θ_A = 110° and minimum θ_R = 40°.

- Comparison of numerical results of Case 3 with the results of Experiment I:

a

0.1 ms

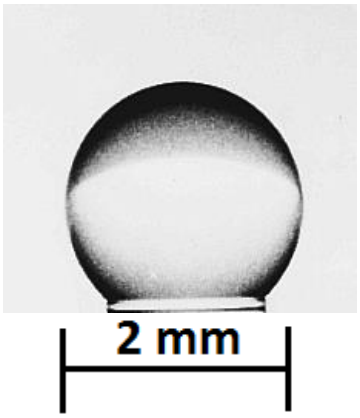

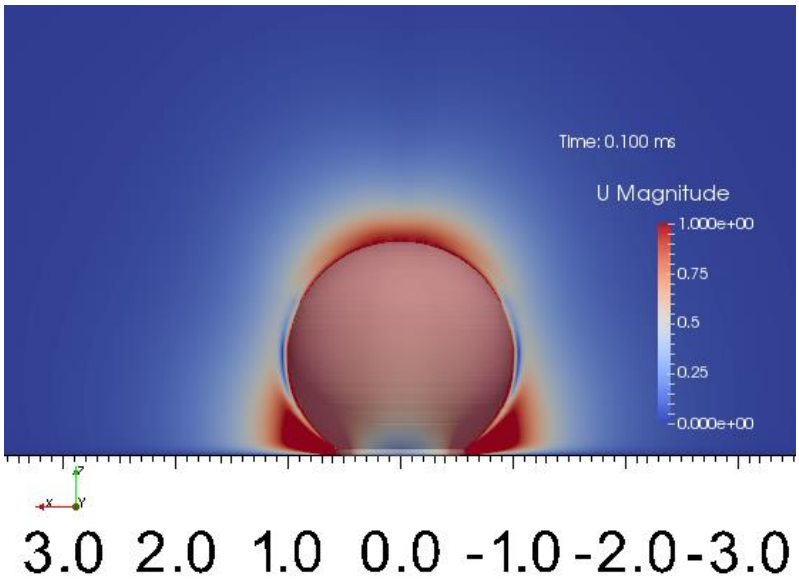

b

0.3 ms

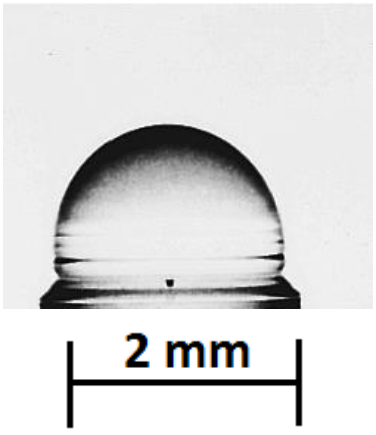

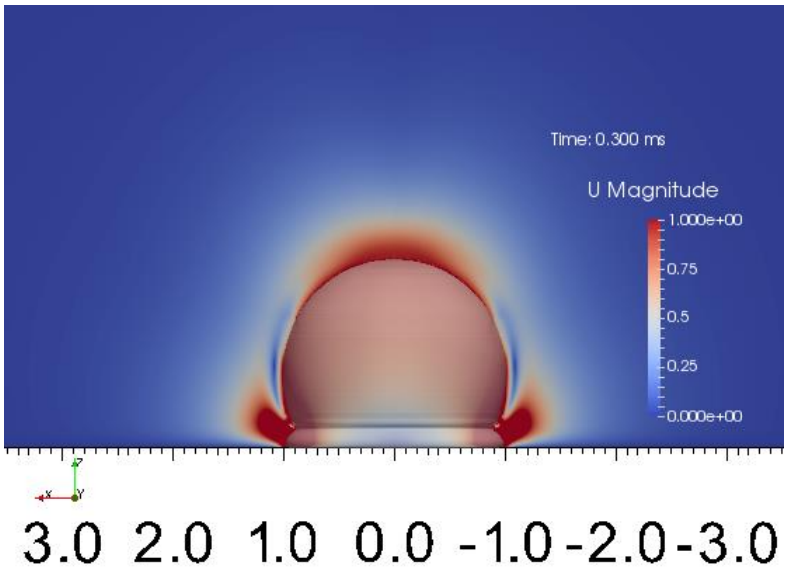

c

1.3 ms

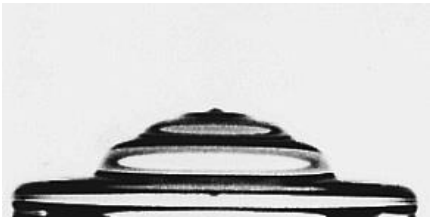

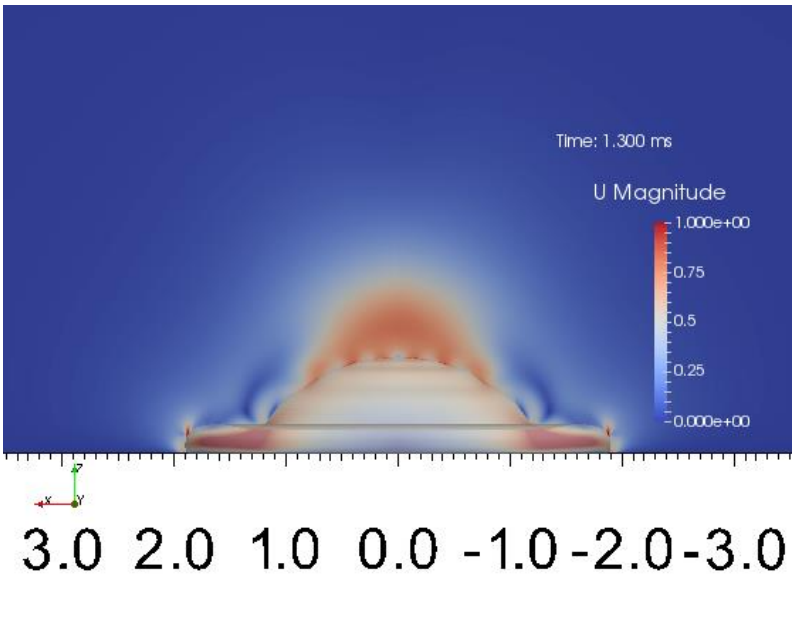

2 mm

d

2.6 ms

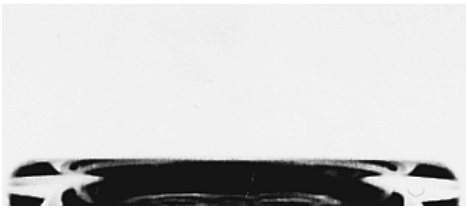

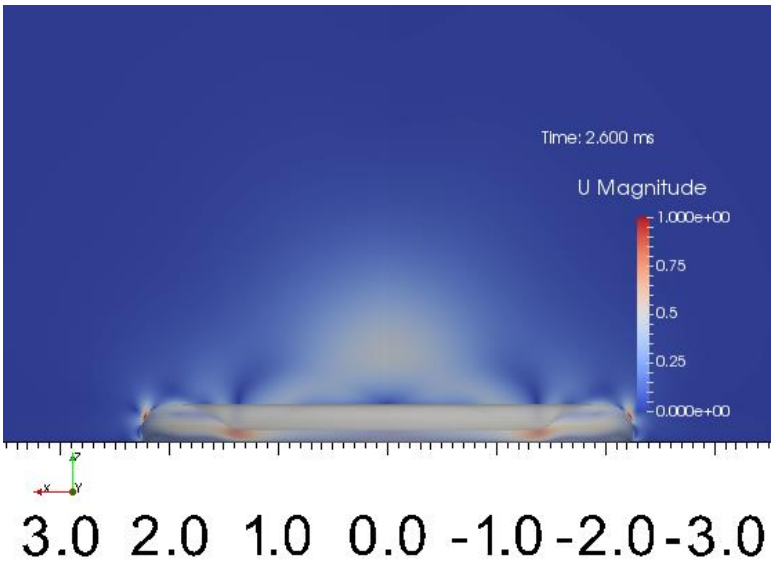

2 mm

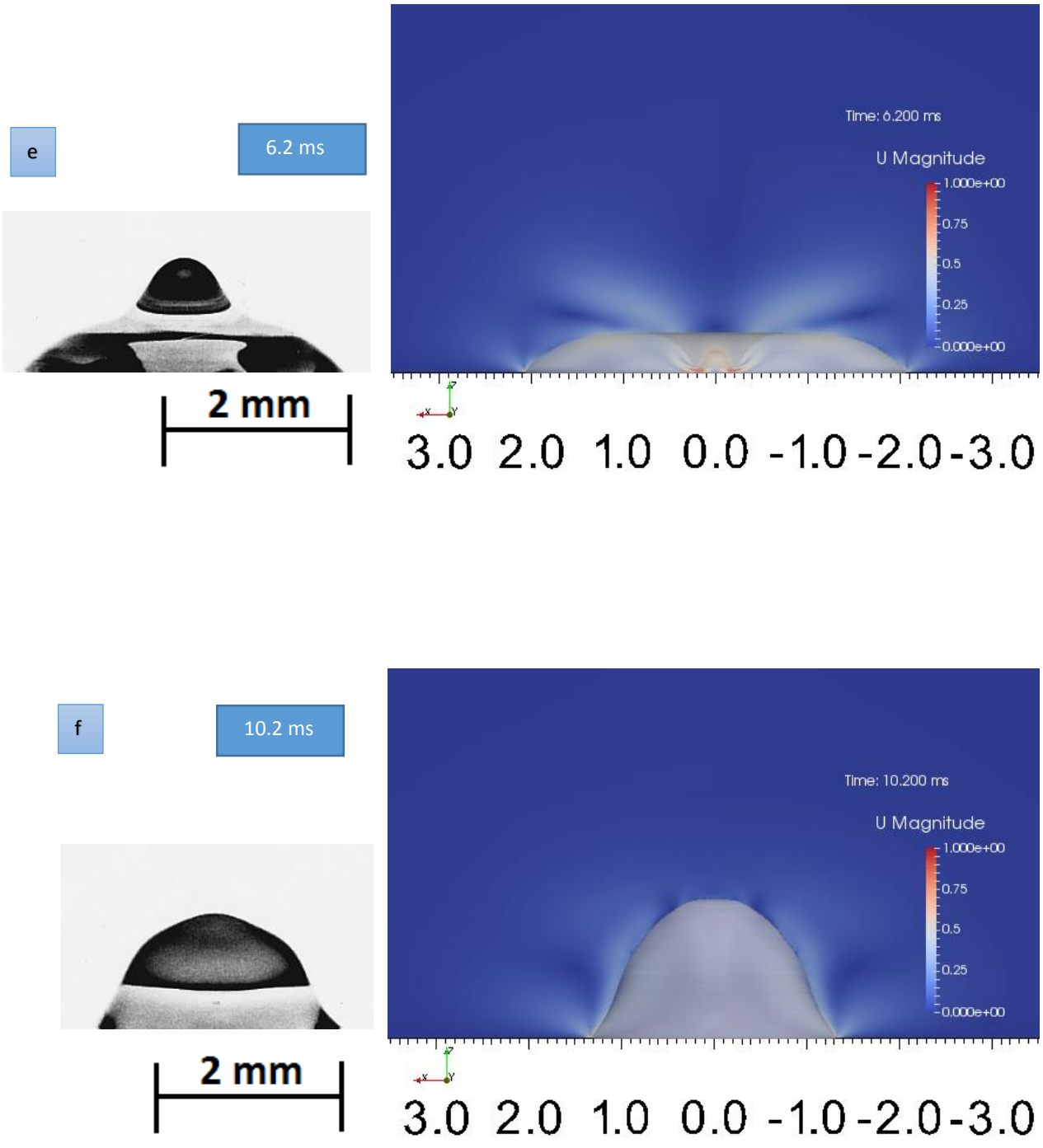

Figure 10: (a,b,c,d,e,f) Spatial and temporal evolution of droplet after the time of impact. Numerical (right) and experimental (left) snapshots.

Comparing to experimental results the dynamicKistlerAlphaContactAngle model shows very good agreement. The biggest difference comparing to experimental results is roughly 0.5mm in the time instance 6.2 ms. Comparing to Case 1 and Case 2, the Kistler's model shows more accurate results not only in the spread of the droplet, but also in the recoiling phase. We can see that in the time instance 10.2ms, where the numerical simulation captures very accurate the experimental results in this particular time instance not only in the shape of the droplet but also in the diameter (<0.2mm difference).

4.2.6 *Comparison of the Experiment I and Numerical results of Cases 1, 2, 3*

Case no.	Equilibrium Contact Angle (°)	Advancing Contact Angle (°)	Receding Contact Angle (°)	Diameter in 0.1ms time instance (mm)	Diameter in 0.3ms time instance (mm)	Diameter in 1.3ms time instance (mm)	Diameter in 2.6 ms time instance (mm)	Diameter in 6.2 ms time instance (mm)	Diameter in 10.2 ms time instance (mm)
Exp.	90	110		1.12	2.05	3.50	4.18	3.58	2.5
1	110	-	-	1.14	1.96	3.78	4.48	2.78	1.12
2	90	110	40	1.20	2.16	4.60	5.44	4.18	1.78
3	90	110	40	1.14	1.96	3.80	4.48	4.14	2.66

Table 1: Maximum wetted droplet diameter of the Experiment I comparing with the results of Constant, Dynamic and dynamicKistler model

As we can see from Table 1, all the numerical simulations up to 0.3 ms shows good agreement with the experimental. After that, dynamicAlphaContactAngle (Case 2) model overpredicts the spreading as well as the recoiling phase of the droplet, resulting pure results in both phases. On the other hand, the results up to 1.3 ms of constantAlphaContactAngle (Case 1) and dynamicKistlerAlphaContactAngle (Case 3) models are significantly better than Case 2. However, after the recoiling phase the difference between the experimental and numerical results started having bigger difference than before with 0.6 mm difference in maximum spreading diameter of the droplet for Case 1 and 0.56 mm for Case 3. Constant CA model continued its pure prediction, resulting 1.13 mm difference with the experimental results in 10.2 ms. Conversely, in the recoiling phase the Kistler's model started predicting more accurate the behavior of the droplet of the experiment reducing its deficit to 0.16mm in the time instance 10.2 ms. Gaph 1 indicates the droplet wetted diameter with respect to time and compares the experimental measurements with the numerical predictions using the Constant, Dynamic and DynamicKistler models. As it can be seen, it is evident that the Kistler model perfoms best with respect to the experimental measurements.

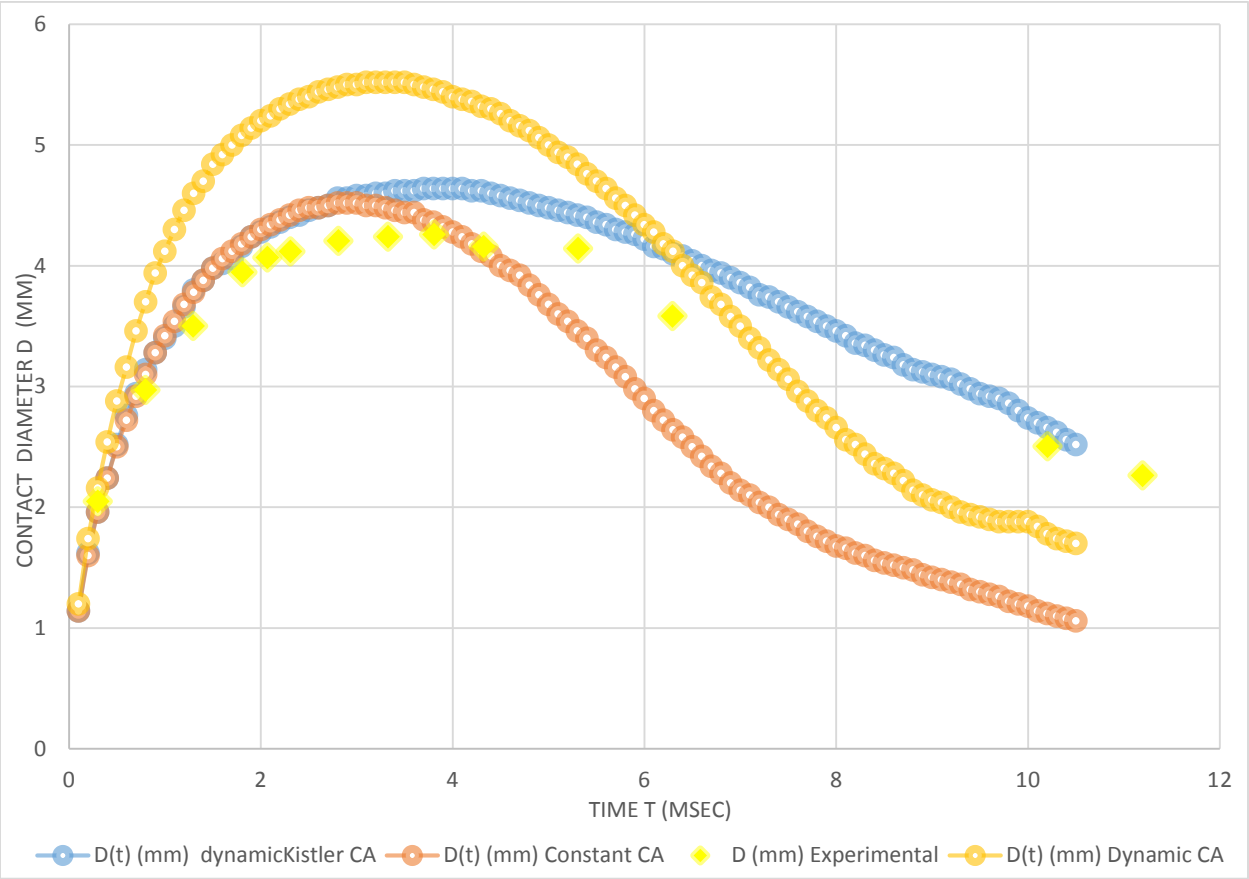

Graph 1: Comparisons of droplet's wetted diameter (D) of experimental results with, Constant, Dynamic and dynamic Kistler contact angle models

In order to visualize better the differences between the 3 different contact angle treatments Figure 10 to 15 below, compares the spatial droplet evolution predictions from the 3 different numerical treatments with respect to the corresponding experimental snapshot, in each of the considered time instances.

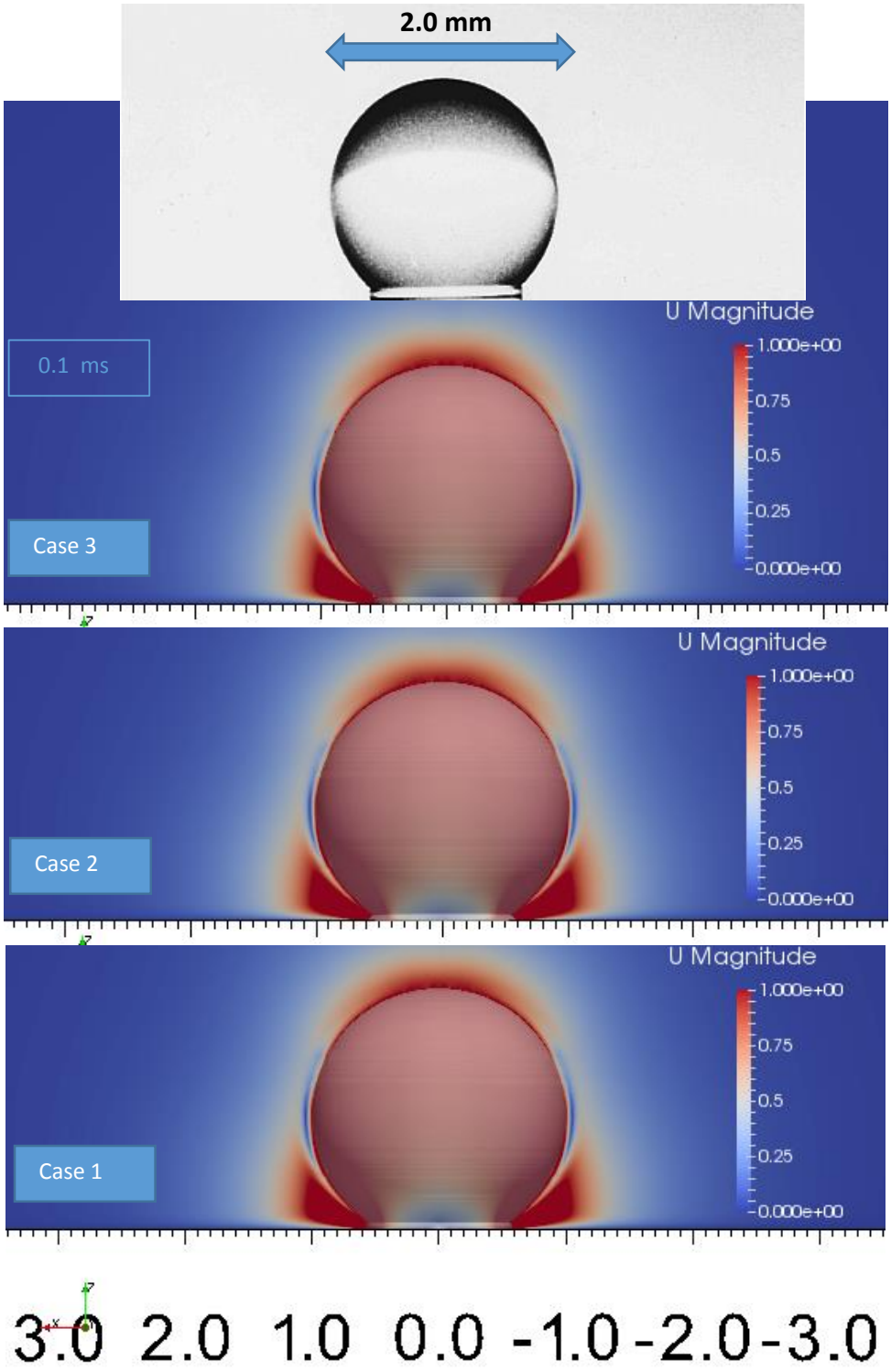

Figure 11: Comparison of the Experiment's I droplet, with the shape and the wetted diameter of the numerical results droplet of all Cases (1,2,3) at the time instance 0.1 ms

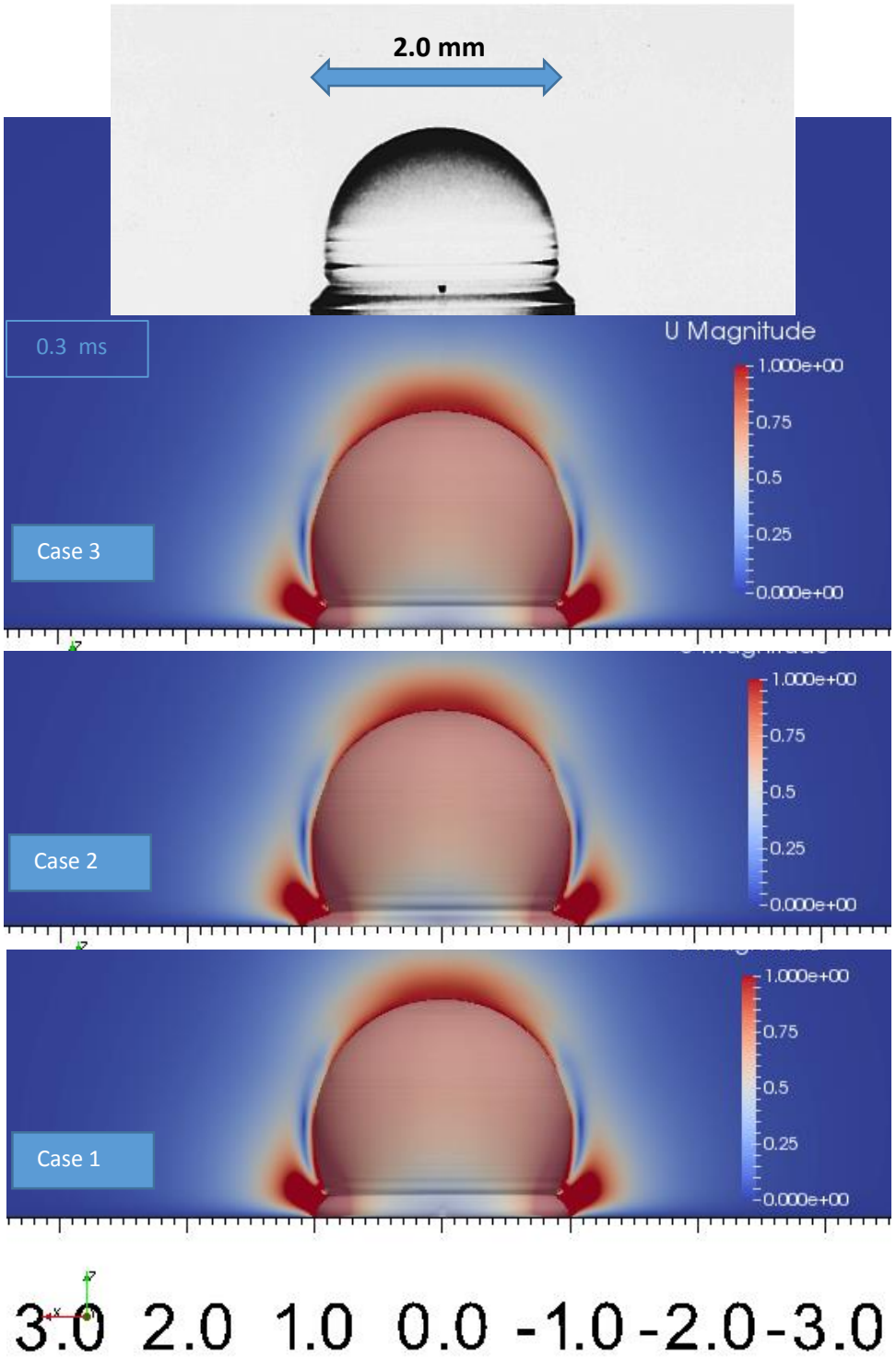

Figure 12: Comparison of the Experiment's I droplet, with the shape and the wetted diameter of the numerical results droplet of all Cases at the time instance 0.3 ms

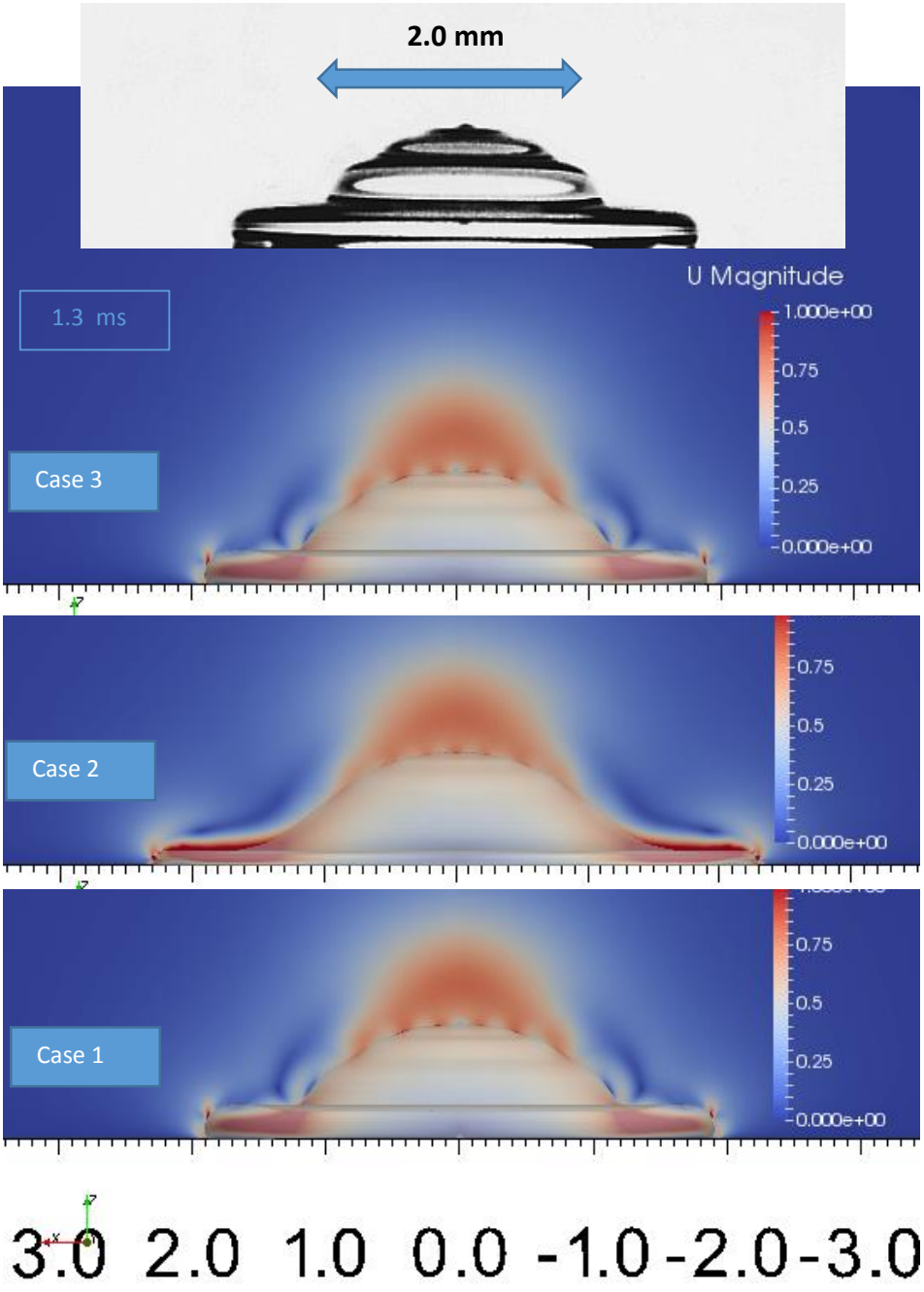

Figure 13: Comparison of the Experiment's I droplet, with the shape and the wetted diameter of the numerical results droplet of all Cases at the time instance 1.3 ms

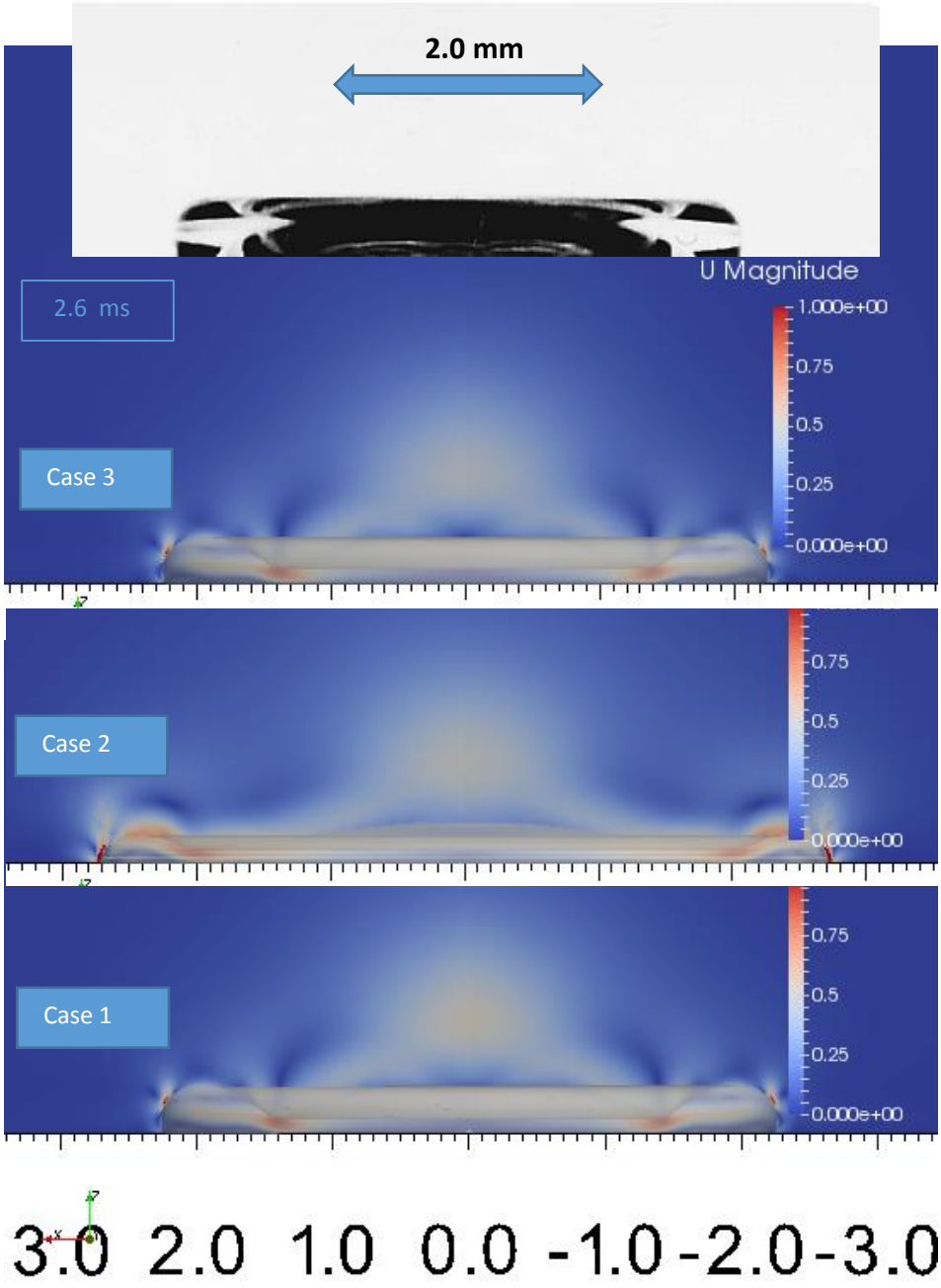

Figure 14: Comparison of the Experiment's I droplet, with the shape and the wetted diameter of the numerical results droplet of all Cases at the time instance 2.6 ms

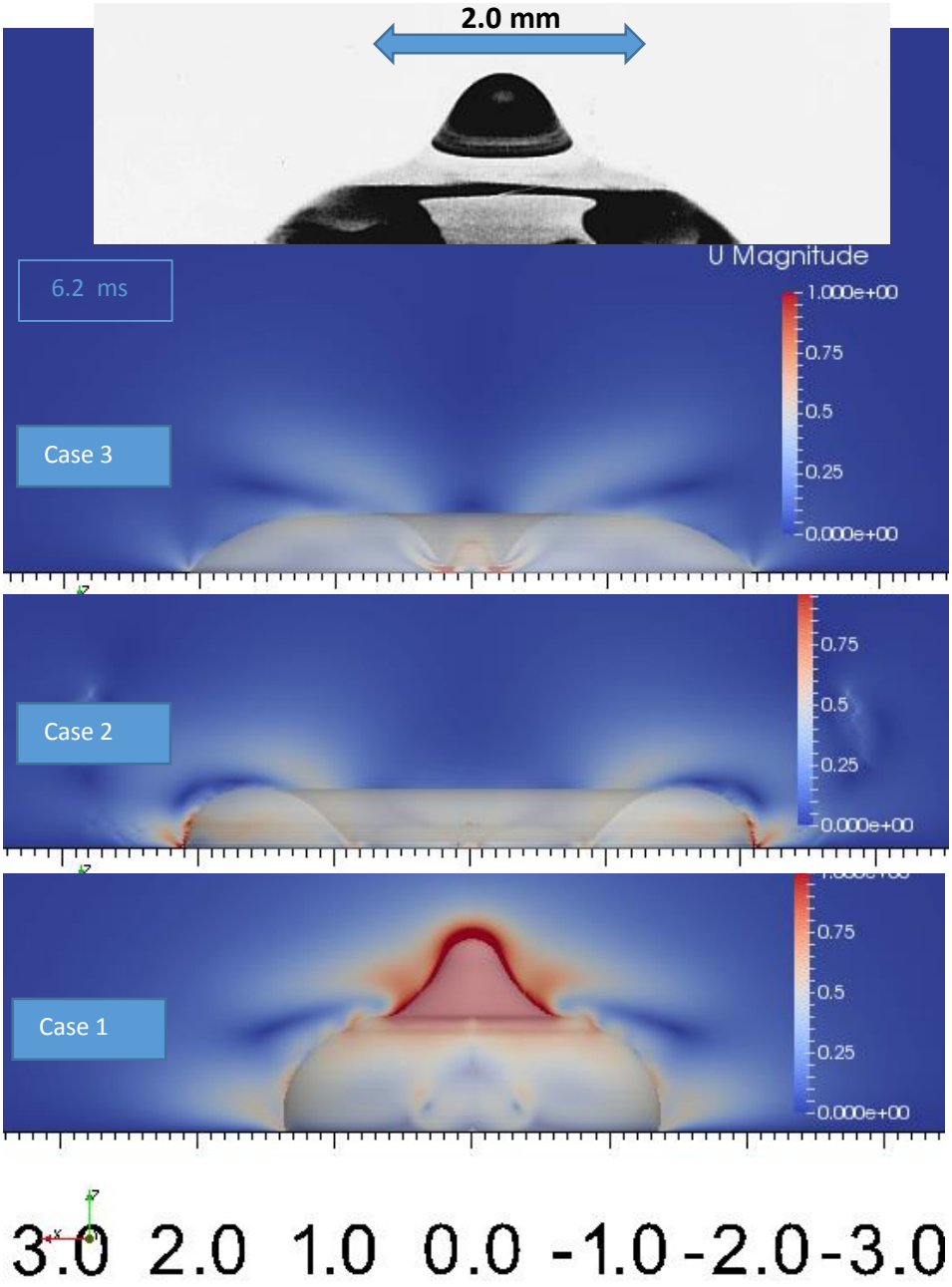

Figure 15: Comparison of the Experiment's I droplet, with the shape and the wetted diameter of the numerical results droplet of all Cases at the time instance 6.2 ms

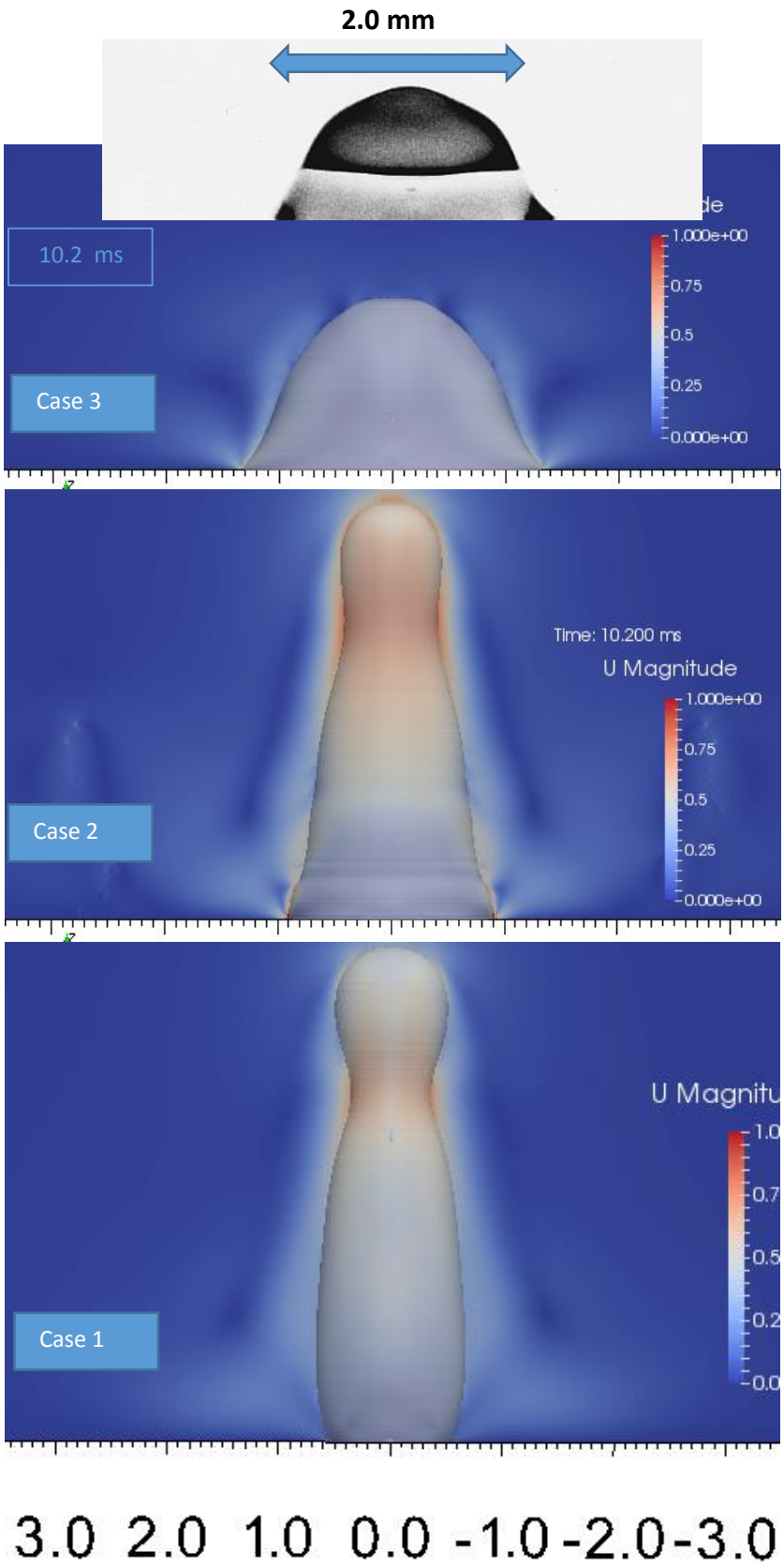

Figure 16: Comparison of the Experiment's I droplet, with the shape and the wetted diameter of the numerical results droplet of all Cases at the time instance 10.2 ms

4.3.1 *Experiment II*

The second experiment investigates droplet impact behavior onto a hydrophobic surface, by Yokoi et al. [5]. Droplets of several millimeters in diameters are generated with a syringe pump connected to a hypodermic needle 150 μm in diameter. Droplets were formed using the pendant drop method. The method generates a droplet by slowly pushing the liquid through the needle until the drop detaches when its weight overcomes the surface tension. This ensures the repeatability of the droplet size as well as of the impact speed which is acquired under gravity. The experimental setup is completed by an optical acquisition system which is combined with adequate drop illumination. It is based on a high speed camera (Nac Memremcam) equipped with a binning option and a 50 W continuous light source. Pictures of 448×338 pixels at a framing rate of 10 000 pictures/s were recorded with a shutter time at 2 μs. Contact diameter and dynamic contact angle measurements were made by automatic image analysis to ensure accuracy (error $\pm$2% for the diameter and $\pm$3° for the contact angle) and avoid human error.
Graph 2 shows the experimental values of contact angle measured during the impact of a 2.28 mm diameter drop arriving at 1 m/s. The properties of the liquid (distilled water) are the following, densities ρ_{water} 1000 $\frac{m^3}{kg}$, ρ_{air} 1.25 $\frac{m^3}{kg}$, dynamic viscosities μ_{liquid} (mu) 1×10^{-3} $\frac{kg}{\sec m}$ μ_{liquid} = 1.82×10^{-5} $\frac{kg}{\sec m}$, surface tension σ =73 $\frac{mNt}{m}$, gravity g = 9.8 $\frac{m}{sec^2}$. The diameter of the droplet D is 2.28 mm and the impact velocity V is 1 m/s.

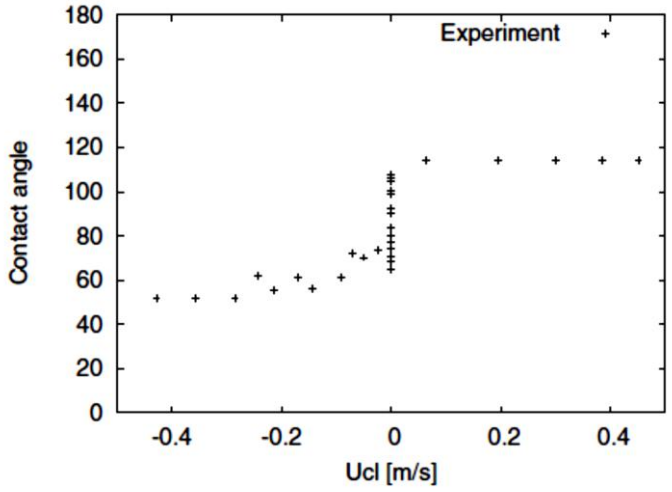

Graph 2: Experimental values of contact angles of droplet impact of Experiment II

4.3.2 *Numerical results with respect of Experiment II*

In this numerical analysis we compiled three cases, one case with Dynamic Contact Angle (Case 4 d), one case with Constant Contact Angle (Case 4 c) and one case with Dynamic Kistler Case (Case 4), however we made comparisons with the experimental results only with the dynamicKistler model, since it is the most accurate model of the three cases. The number of cells is 1.6 million (1000 × 1600 × 1). In the directories of the OpenFOAM folders we used the same parameters as the experiment by Yokoi et al. [5], also the droplet diameter is 2.28 mm and the impact velocity of the droplet is 1 m/s.

4.3.3 Case 4

As we said before in this case we are using the dynamicKistlerAlphaContactAngle model. The values of contact angles that are specified in the proposed model are, of θ_{eq} = 90°, θ_A = 107°, θ_R = 77°

- Comparison of numerical results of Case 4 with the results of Experiment II:

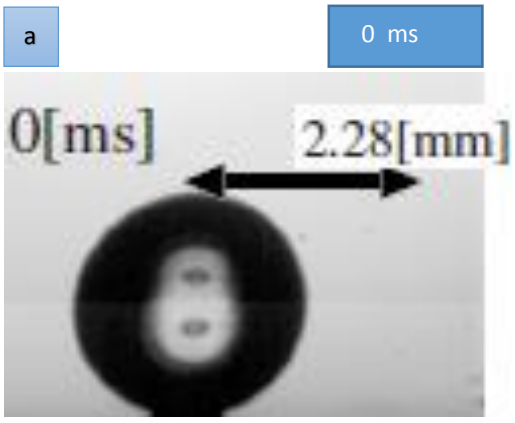

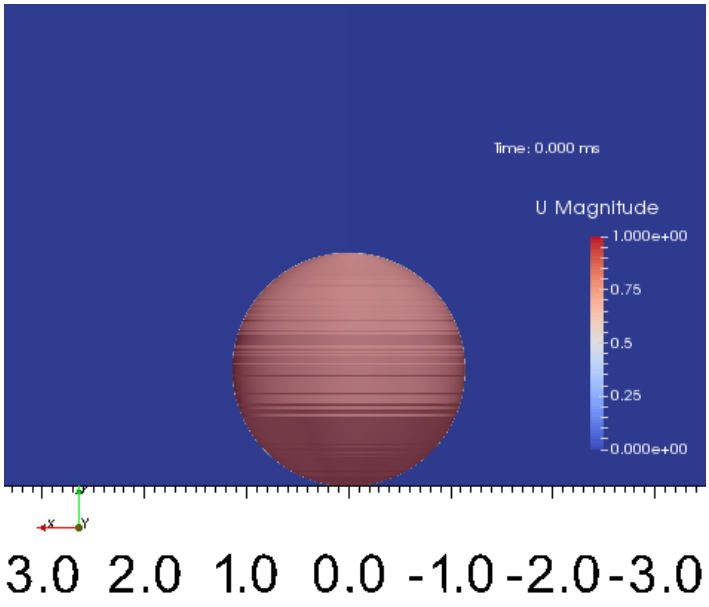

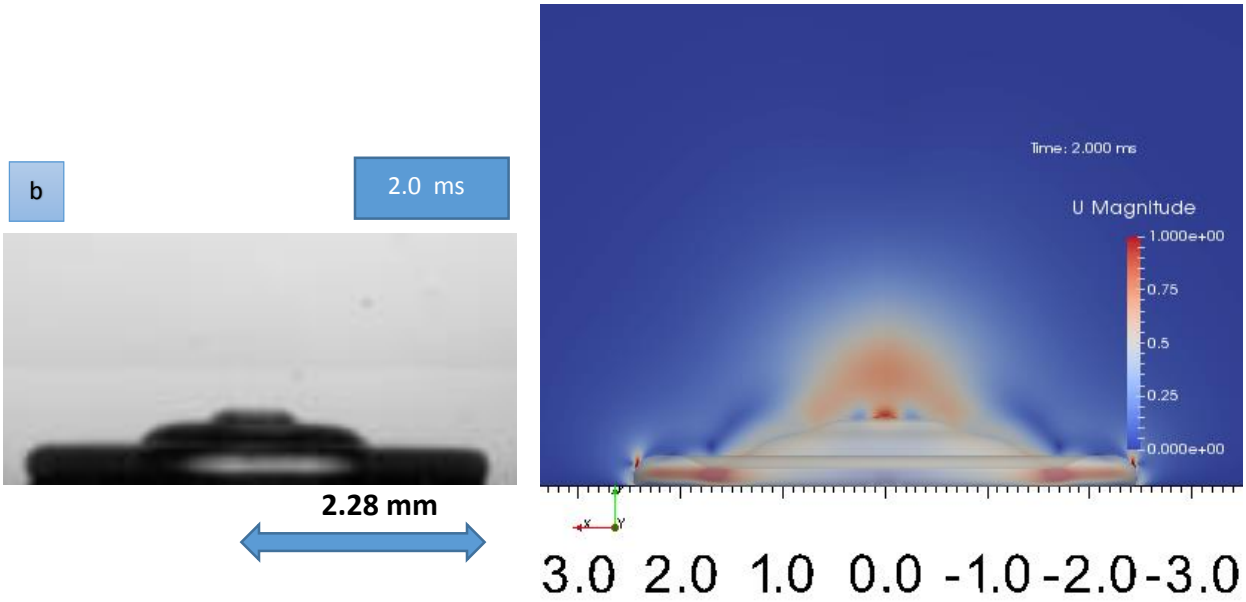
b
2.0 ms
2.28 mm
Time: 2.000 ms
U Magnitude
1.000e+00
0.75
0.5
0.25
0.000e+00
3.0 2.0 1.0 0.0 -1.0 -2.0 -3.0

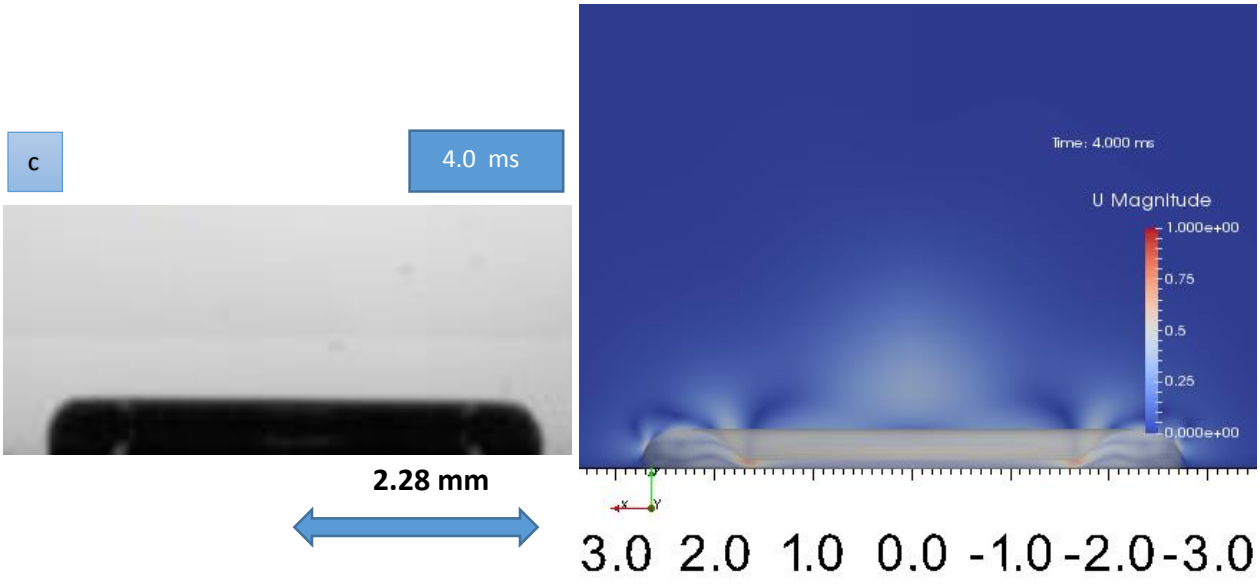
c
4.0 ms
2.28 mm
Time: 4.000 ms
U Magnitude
1.000e+00
0.75
0.5
0.25
0.000e+00
3.0 2.0 1.0 0.0 -1.0 -2.0 -3.0

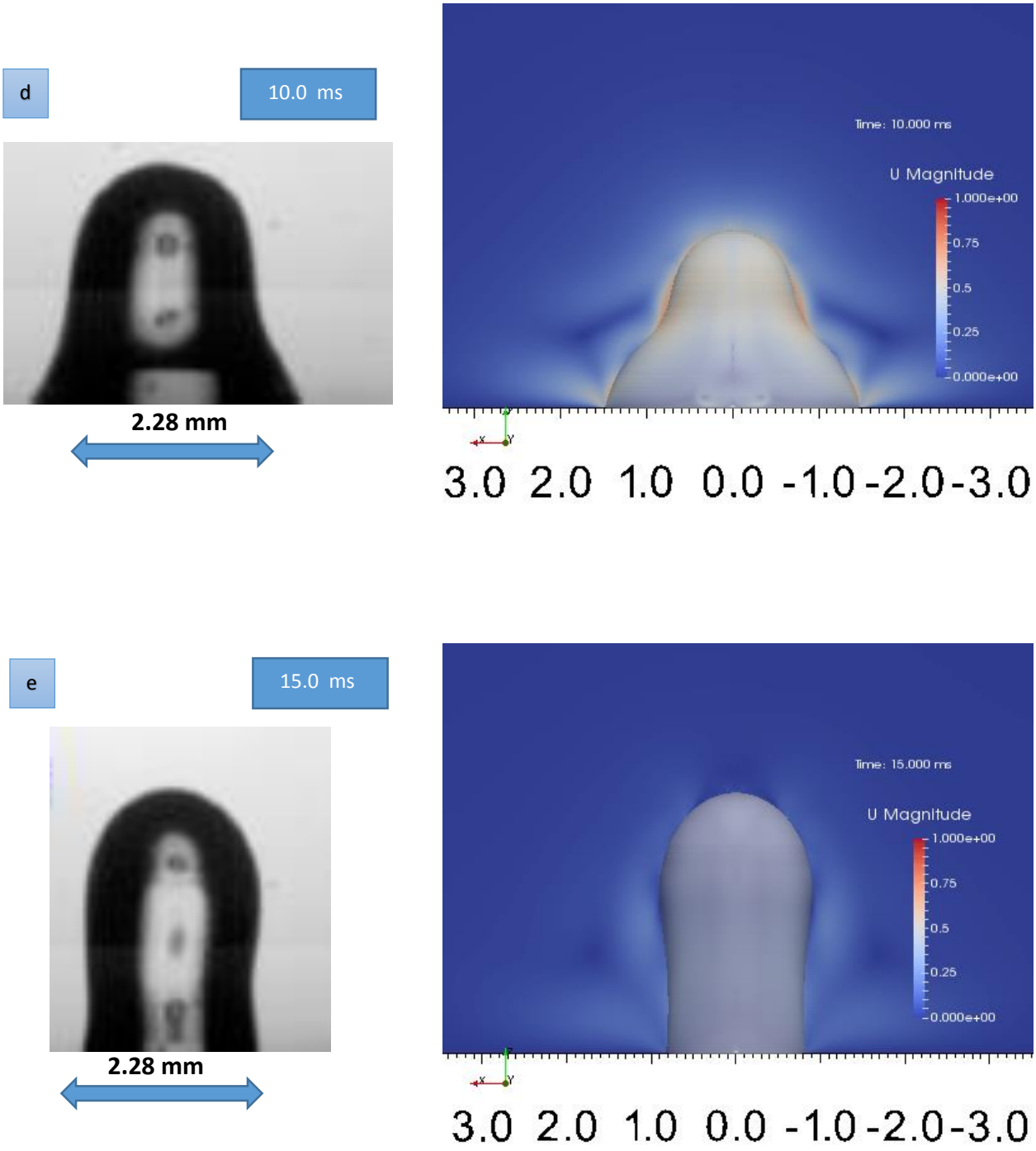

Figure 17: (a,b,c,d,e) Spatial and temporal evolution of droplet after the time of impact. Numerical (right) and experimental (left) snapshots.

We did numerical simulations of a 2.28 mm distilled water and 1 m/s velocity. The above figure is a comparison of the experiment by Yokoi et el. [5], and the dynamicKistlerAlphaContactAngle model of OpenFOAM 2.2.1. The numerical simulation shows very accurate results comparing to experimental. Up to 2 ms the difference of the wetted droplet diameter is less than 0.2 mm (<0.2 mm). After the maximum spreading and in the recoiling phase the numerical simulations continuous to show very good agreement, with wetted diameter difference to be roughly 0.4mm.

4.3.4 *Comparison of the Experiment I and Numerical results of Cases 4, 4c, 4d*

In order to have more data to compare with the experimental results of the droplet impact, apart from the dynamicKistlerAlphaContactAngle model we also run simulations of the dynamicAlphaContactAngle and the constantAlphaContactAngle models. The results are demonstrated in the Table 2 and in the Graph 3.

Case no.	Equilibrium Contact Angle (°)	Advancing Contact Angle (°)	Receding Contact Angle (°)	Diameter in 0 ms time instance (mm)	Diameter in 2.0 ms time instance (mm)	Diameter in 4.0 ms time instance (mm)	Diameter in 10.0 ms time instance (mm)	Diameter in 15.0 ms time instance (mm)
Exp.	90	107	77	0	4.62	5.18	3.29	2.06
4	90	107	77	0	4.80	5.48	2.98	1.64
4c	90	-	-	0	5.20	6.04	2.80	N/D
4d	90	107	77	0	5.58	6.20	N/D	N/D

Table 2: Maximum wetted droplet diameter of the Experiment II comparing with the results of Constant, Dynamic and dynamicKistler's model

Table 2 and Graph 3, shows the difference of the wetted diameter of the droplet impact on hydrophobic surface. As it is expected the Kistler's models shows the most accurate results comparing to experimental. In more detail, up to 10.0 ms the biggest difference (0.31 mm) is in the maximum spreading diameter of the drolet (4.0 ms), however when the recoil of the droplet starts and after that, the numerical simulation of OpenFOAM shows even more accurate results with the experimental. Regarding constantAlphaContactAngle and dynamicAlphaContactAngle models, the results are as expected. The Constant contact angle model shows more accurate

results than the Dynamic contact angle model, but less accurate than the dynamicKistler model. The biggest difference comparing to experimental results is in maximum diameter of the droplet which for dynamic was 6.04 mm (0.86 mm bigger that the experiment diameter), however in the recoiling phase the constant contact angle model shows good agreement (0.49 mm less than the experimental) with the experiment. The dynamic contact angle model as it is referred before it is the least accurate model of the three, the reason is the definition of an empirical value called velocity scale, which has always value 1 in the alpha1 directory of OpenFOAM. Up to 0.5ms the model shows good agreement with the experimental results, however after that the dynamic model overpredicted the wetted diameter of the droplet, resulting maximum diameter in the 4.0ms time instance of 6.2 mm (1.0mm higher than the experimental value). In the recoiling phase, the accuracy was better than the maximum spreading diameter of the droplet, with maximum deficit of about 0.5 mm less than the experimental wetted diameter.

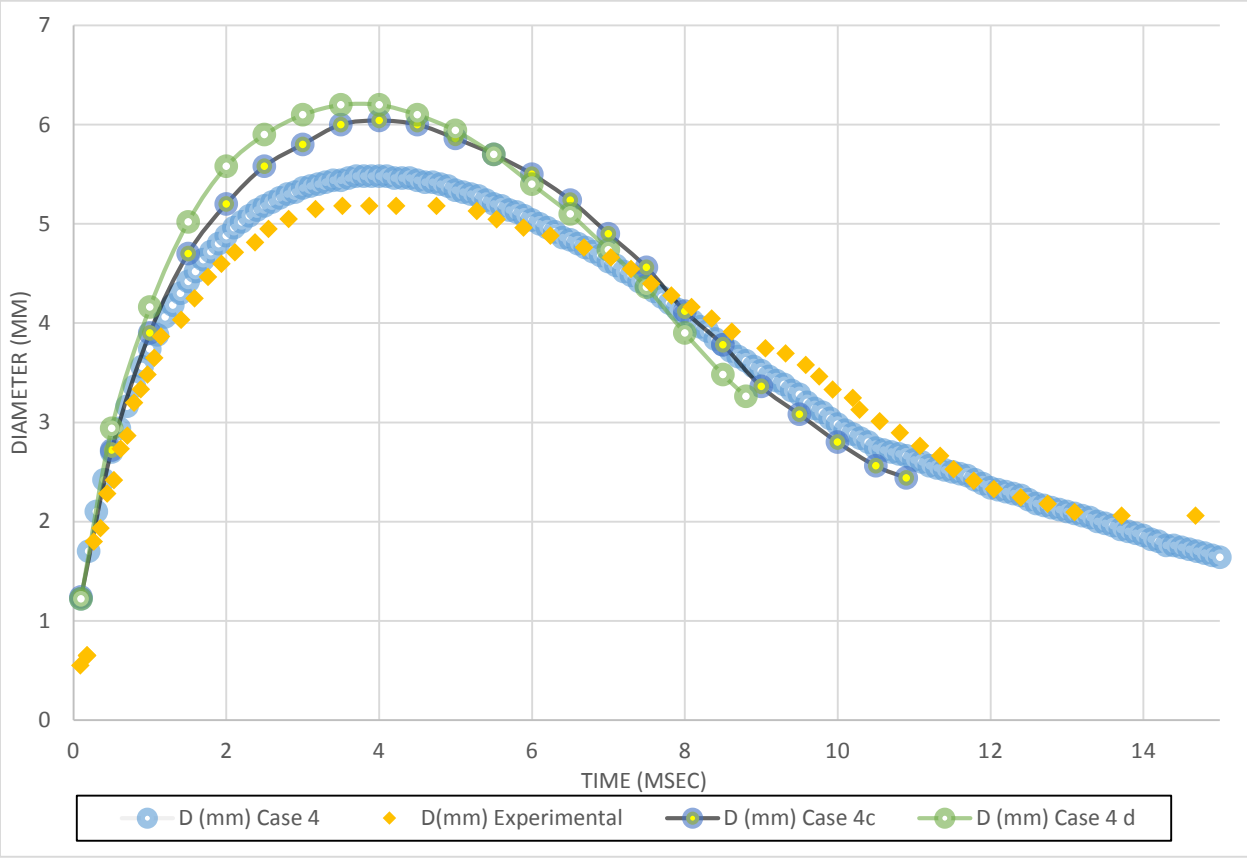

Graph 3: Comparisons of wetted diameter (D) of experimental results with, Constant, Dynamic and dynamic Kistler contact angle models

4.4.1 *Experiment III*

The next experiment is done by Patil et al. (2016) [6], in micropillared surface. The micropillared surfaces were fabricated using an ultraviolet lithography technique, after depositing SU-8 (2025) epoxy polymer on a 2 inch silicon wafer. The surfaces are coated with 10 nm platinum layer. The SEM images of the fabricated micropillared surface, with 47 µm pitch, are shown in Fig.4a. The measured width and height of the square pillars are 20 ±2 µm and 27 ± 2 µm, respectively. In this experiment, microliter water droplets of 1.7 ± 0.05 mm diameter are generated using microsyringe and impacted on the surface. The height of the needle is adjustable to vary the impact velocity. Droplets are visualized (from the side) using a high-speed camera (MotionPro, Y-3 classic, CMOS, C-mount) with long distance working objective (Qioptiq Inc.) , similar to the setup in Refs. Bhardwajand Attinger (2008) [29] and Bhardwajetal et al. (2010) [30]. The images of 192 × 632 pixels at 1500 fps (with an exposure time of 330 µs) are captured. To measure the equilibrium contact angle on the surface, a droplet is gently deposited on the surface and equilibrium contact angle is measured after it assumes a shape of spherical cap. The measured equilibrium contact angle for the present micropillared surface is θeq=147°. Furthermore, the advancing (θadv=161°) and receding (θrec=132°) contact angles are measured by tilting the surface with droplet kept on it, as done by Bhushan et al. (2009) [7]. The uncertainty in the contact angle measurements was ±3°. The experiments were performed with adeionized (DI) water in a con-trolled environment, with temperature as 25 ± 1°C and relative humidity as 38 ± 5 %. Since the equilibrium contact angle θ_{eq} is 147°, the surface is hydrophobic.

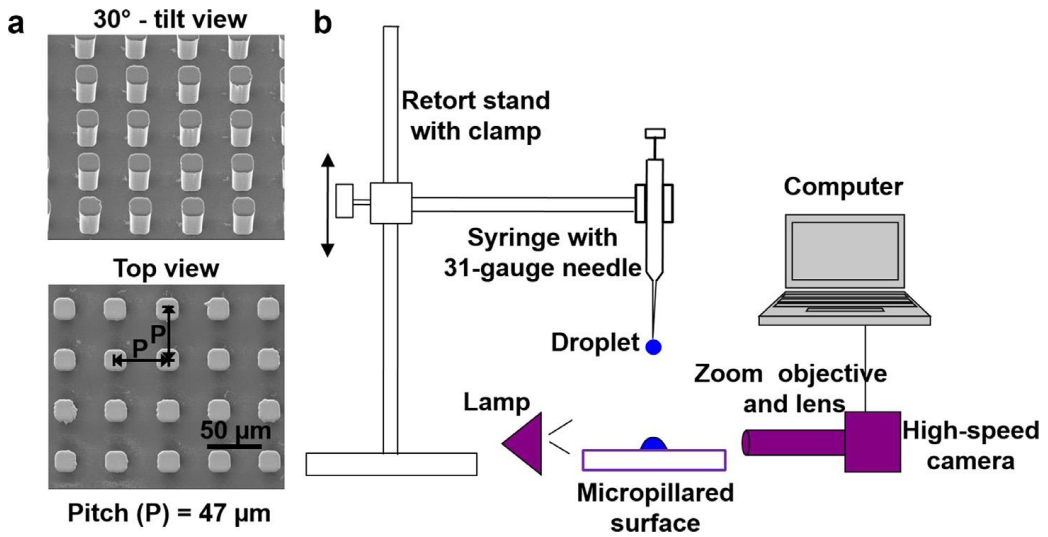

Figure 18: (a) SEM images of micropillared surface with 47 µm pitch of uniformly-spaced square pillars of 20 µm width and 27 µm height; and (b) schematic of the experimental setup, by Patil et al. [7]

4.4.2 *Numerical results with respect of Experiment III*

We will name this numerical simulation Case 5. In this case we will compare the experimental data by Patil et al. [6] with the dynamicKistlerAlphaContactAngle model only, since as it is proved in literature [20] and also from the previous comparisons in this dissertation, is the most accurate and reliable boundary condition. The number of cells is 1.6 million ($1000 \times 1600 \times 1$). In the directories of the OpenFOAM folders we used the following parameters (densities ρ_{water} 1000 $\frac{m^3}{kg}$, ρ_{air} 1.25 $\frac{m^3}{kg}$, dynamic viscosities μ_{liquid} (mu) 1×10^{-3} $\frac{kg}{\sec m}$, μ_{liquid} = 1.82×10^{-5} $\frac{kg}{\sec m}$, surface tension σ =73 $\frac{mNt}{m}$, gravity g = 9.8 $\frac{m}{sec^2}$). The droplet diameter is 1.7 mm and the impact velocity is also the droplet diameter is 2.28 mm and the impact velocity of the droplet is 0.34 m/s [6].

4.4.3 Case 5

Only the dynamicKistlerAlphaContactAngle model will be compared with the experiment III. The values of contact angles are, of θ_{eq} = 147°, θ_{Adv} = 161°, θ_{Rec} = 132°.

The following pictures are the numerical results of the Case 5 (right side), compared with photographs (left side) of the experiment by Patil et al. [6]:

- Comparison of numerical results of Case 5 with the results of Experiment III:

a

0.0 ms

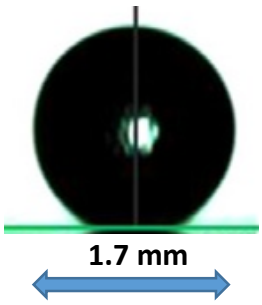

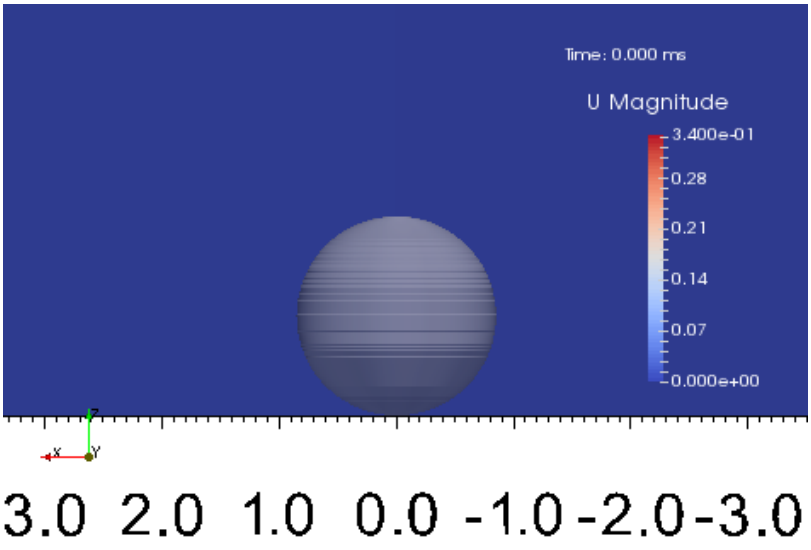

b

2.00 ms

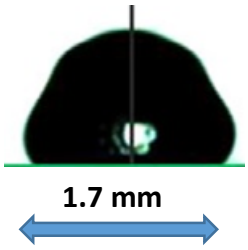

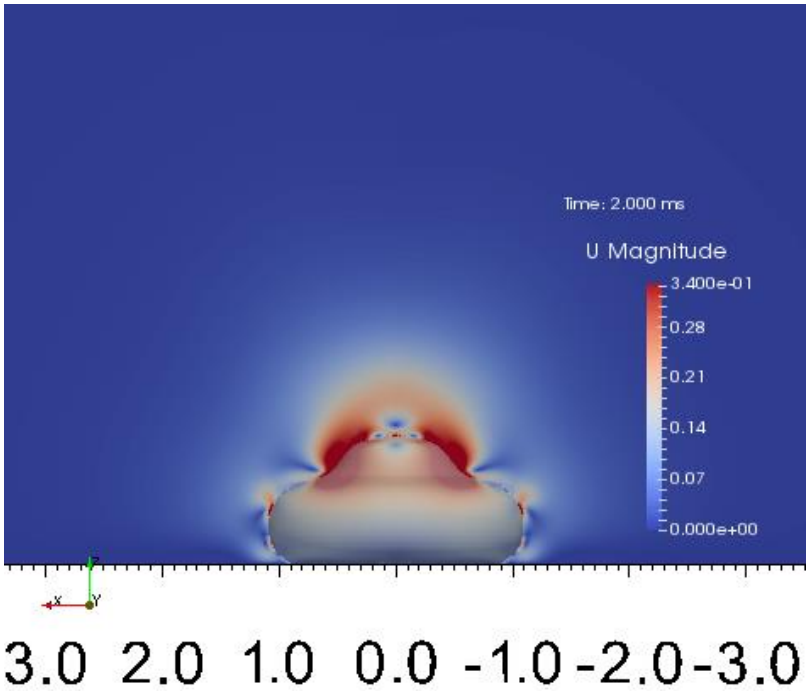

c

4.00 ms

1.7 mm

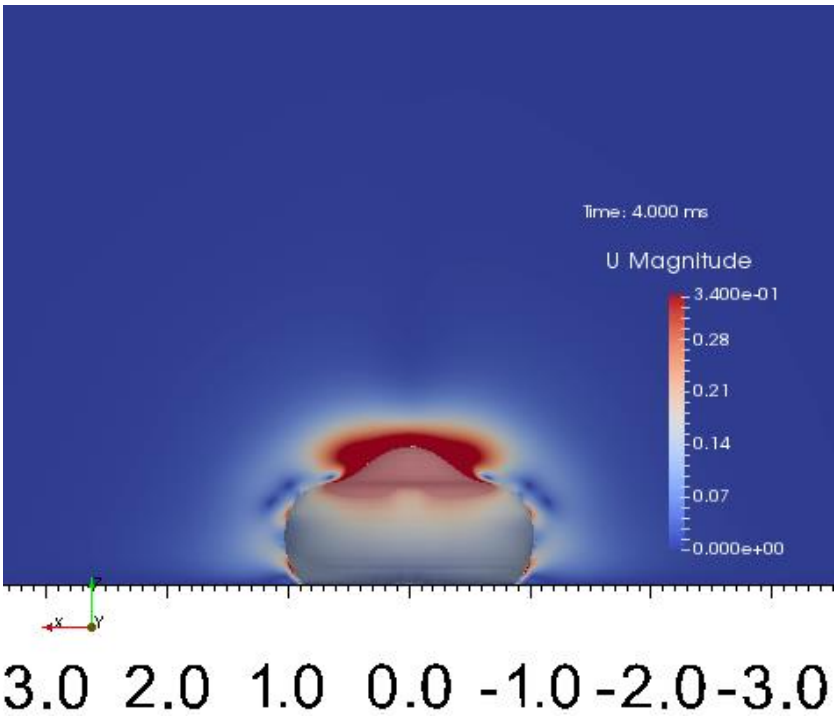

d

8.67 ms

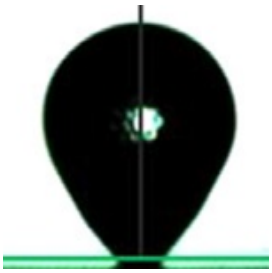

1.7 mm

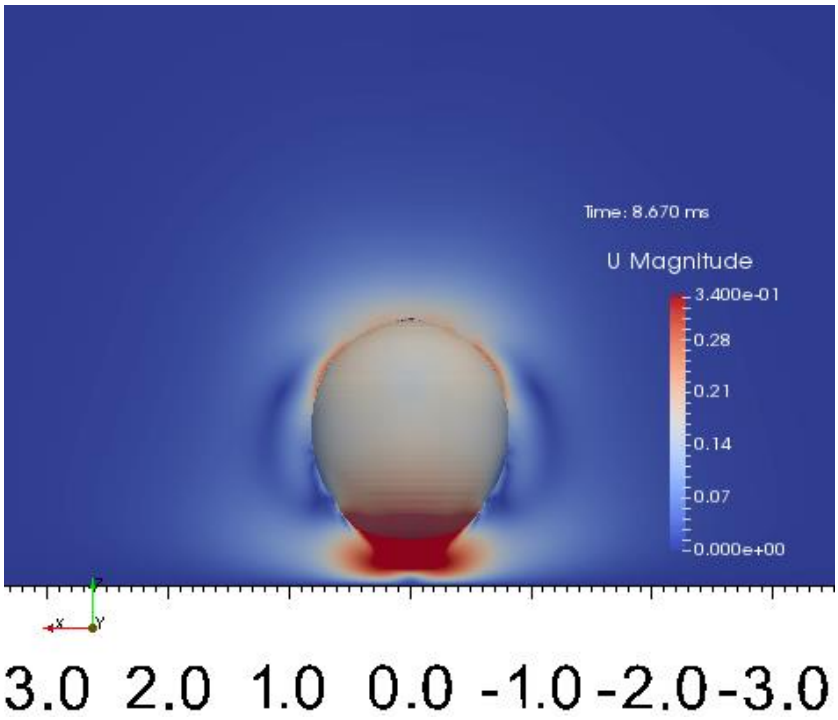

e

9.33 ms

1.7 mm

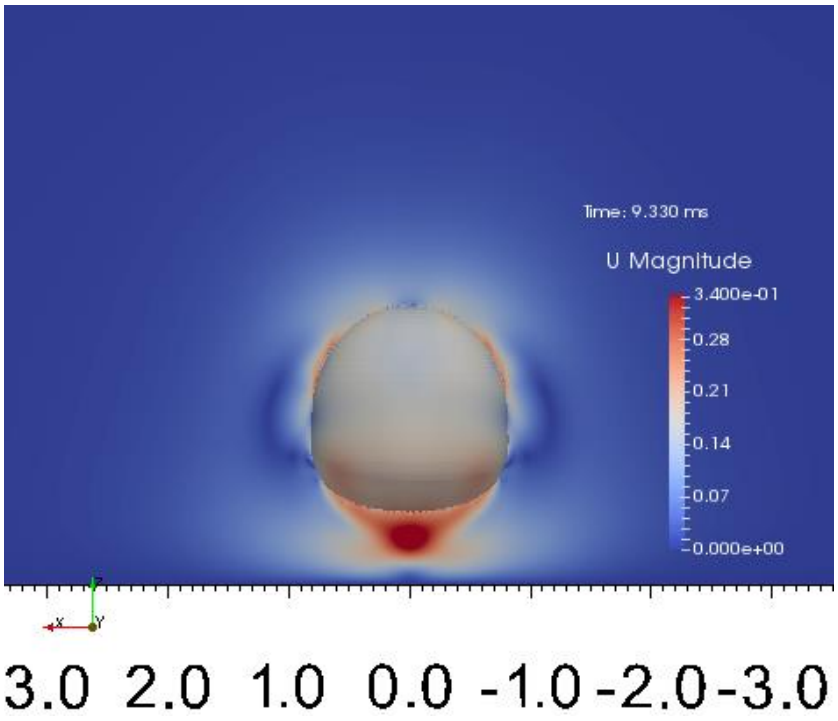

f

10.67 ms

1.7 mm

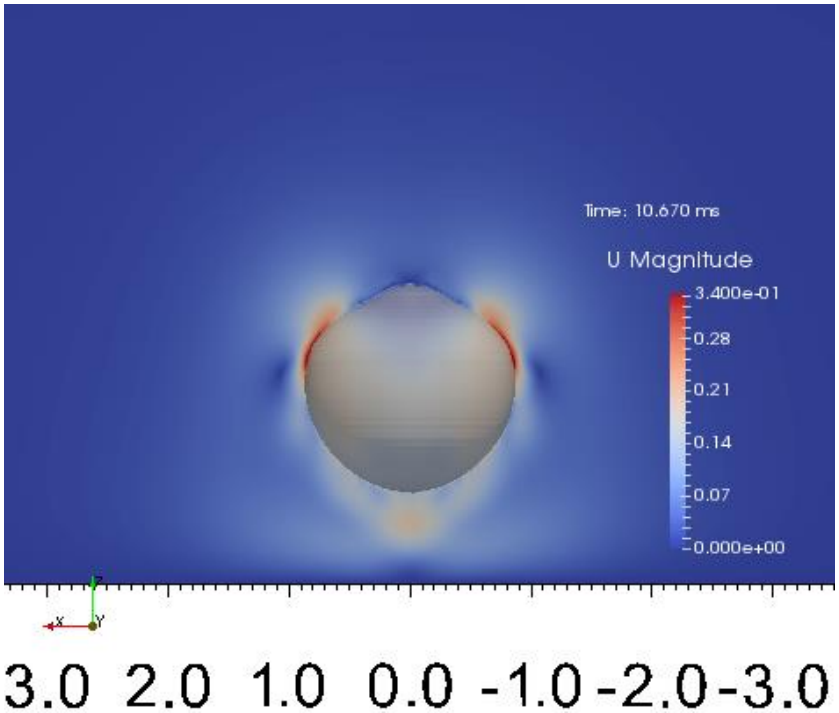

g

12.00 ms

1.7 mm

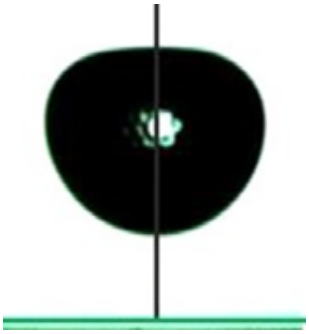

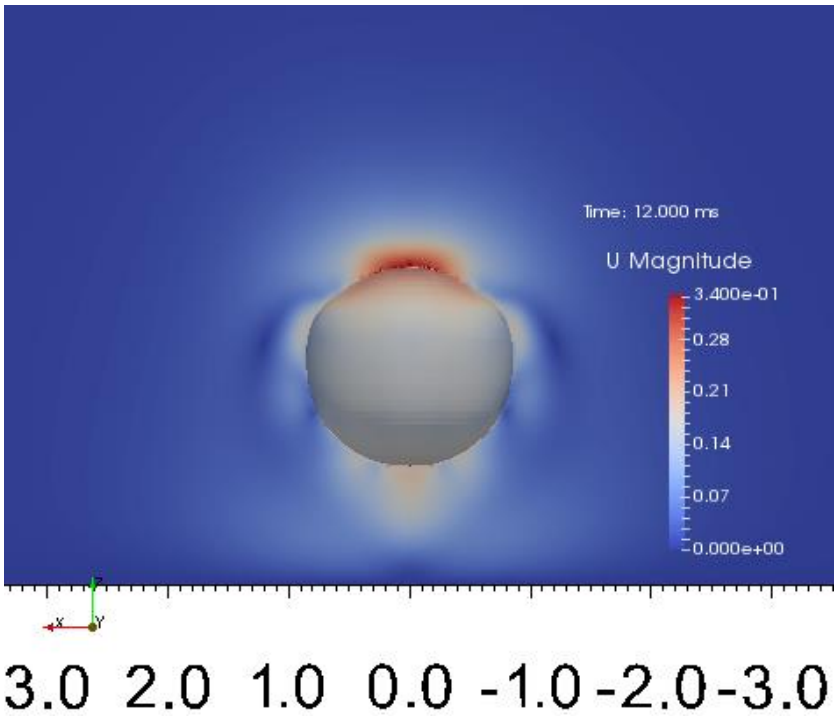

h

14.00 ms

1.7 mm

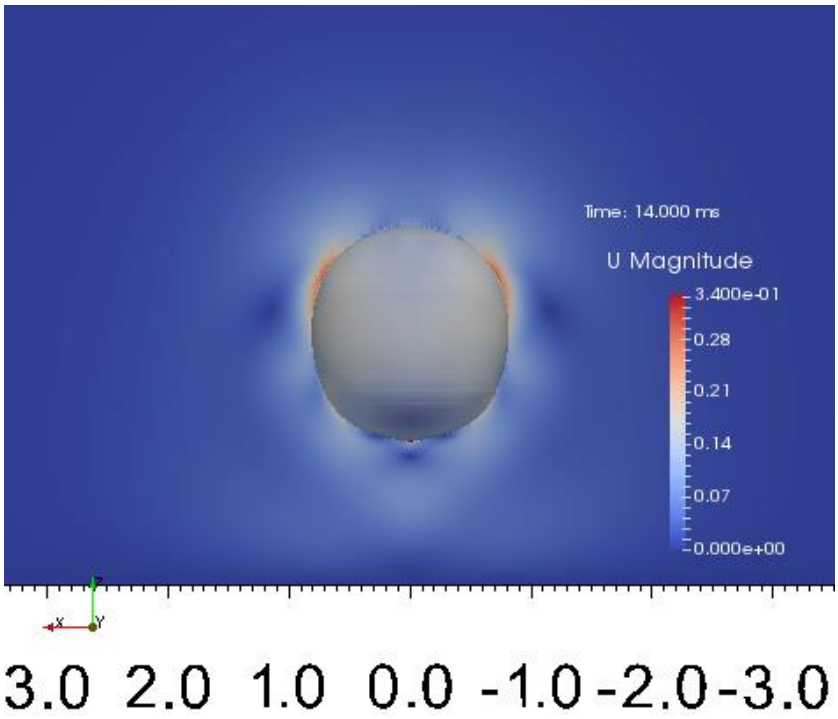

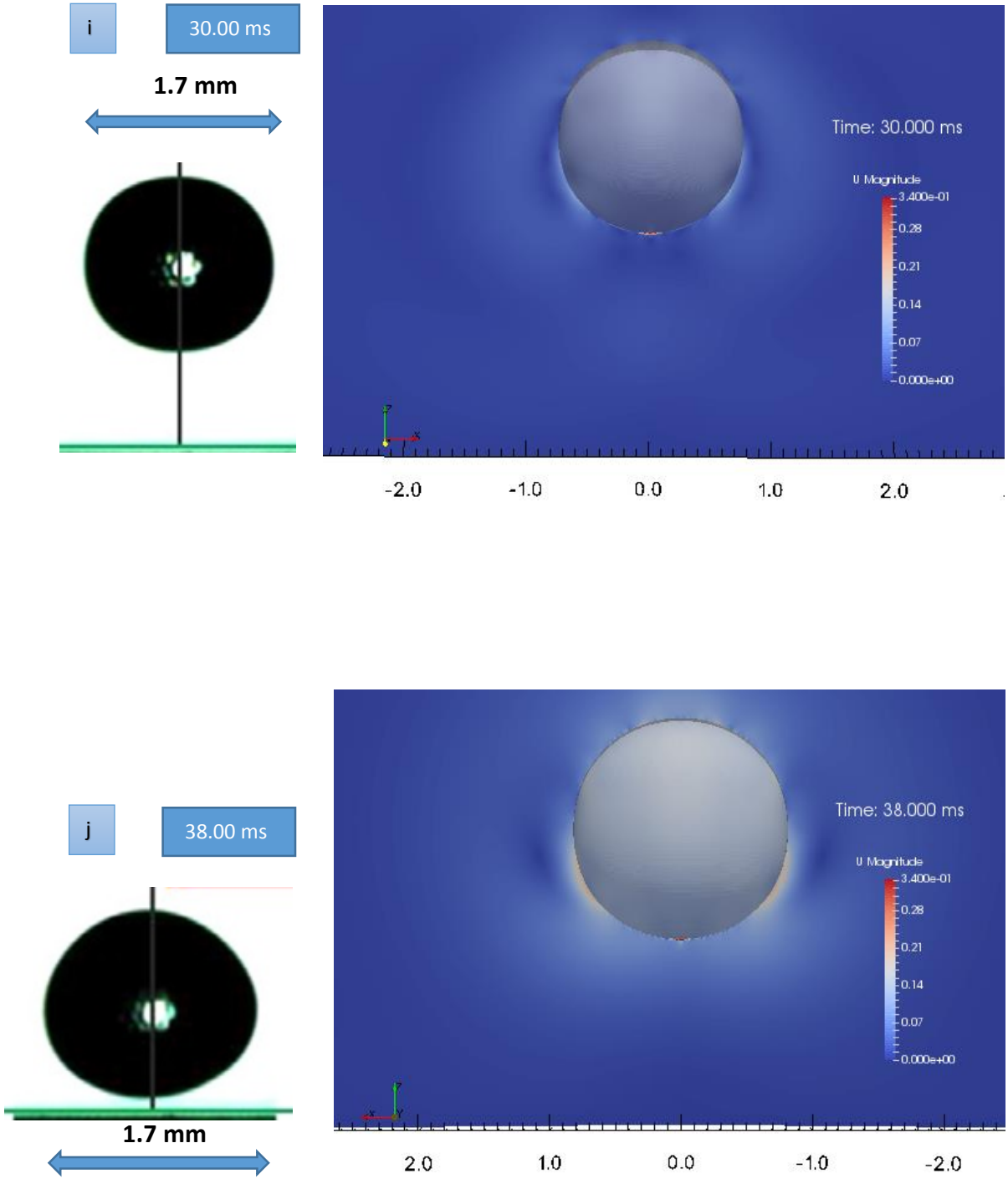

Figure 19: (a, b, c, d, e, f, g, h, i, j) Spatial and temporal evolution of droplet after the time of impact. Numerical (right) and experimental (left) snapshots.

4.4.4 *Comparison of the Experiment III and Numerical Results of CASE 5*

The above figures compare experimental results [7] of droplet impact, with numerical results using the dynamicKistlerAlphaContactAngle of OpenFOAM. The diameter of the droplet is 1.7 mm and the impact velocity is 0.34 m/s on hydrophobic surface. Both in spreading as well as in recoiling phase of the numerical simulation the results show very good agreement with the experimental results. Up to 9.33 ms we can see that the numerical simulation is going about 0.6 ms faster than the experimental results. After the detachment of the droplet up to 14 ms numerical and experimental results are showing perfect agreement. After that the droplet in the experiment seems to go faster comparing to the numerical, so while in the numerical simulation at the 30.0 ms the droplet is in its higher distance from the surface, in the experiment the droplet has already begun approaching the surface.

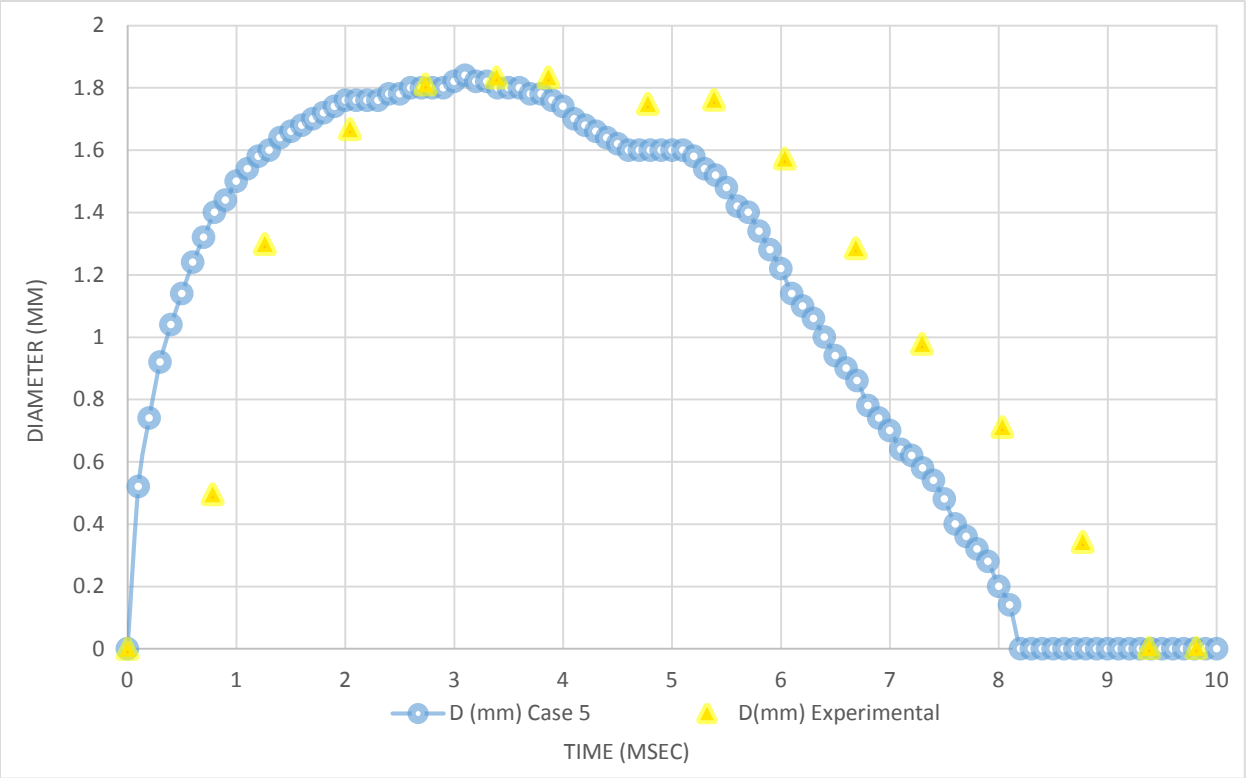

Graph 4: Comparisons of droplet's wetted diameter (D) of the Experiment III, with dynamicKistler contact angle model

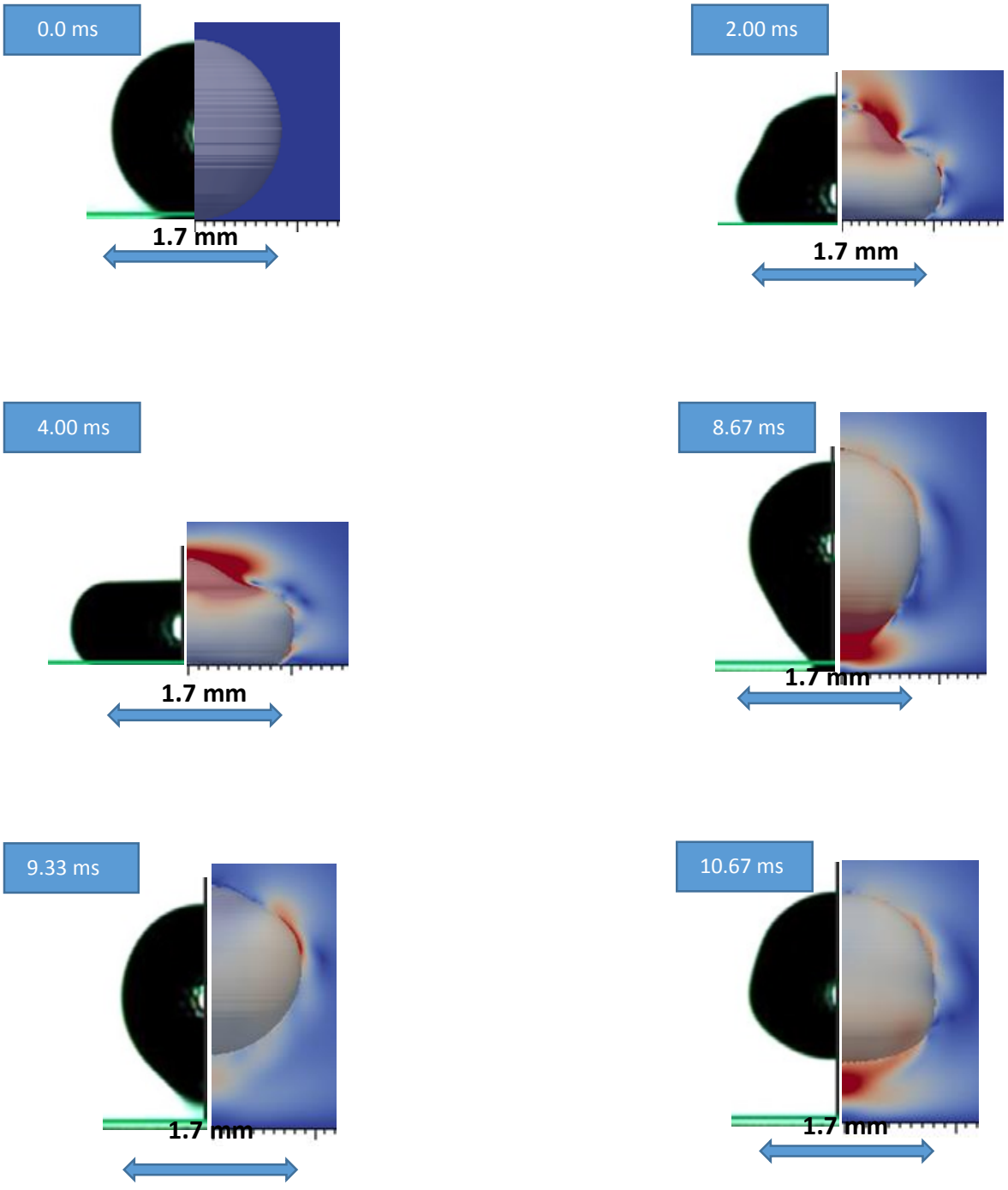

Figure 20: Comparison of Experiment's droplet shape (right side), with numerical simulations results of dynamicKistler' s model in different time instance (0 ms to 10.67 ms)

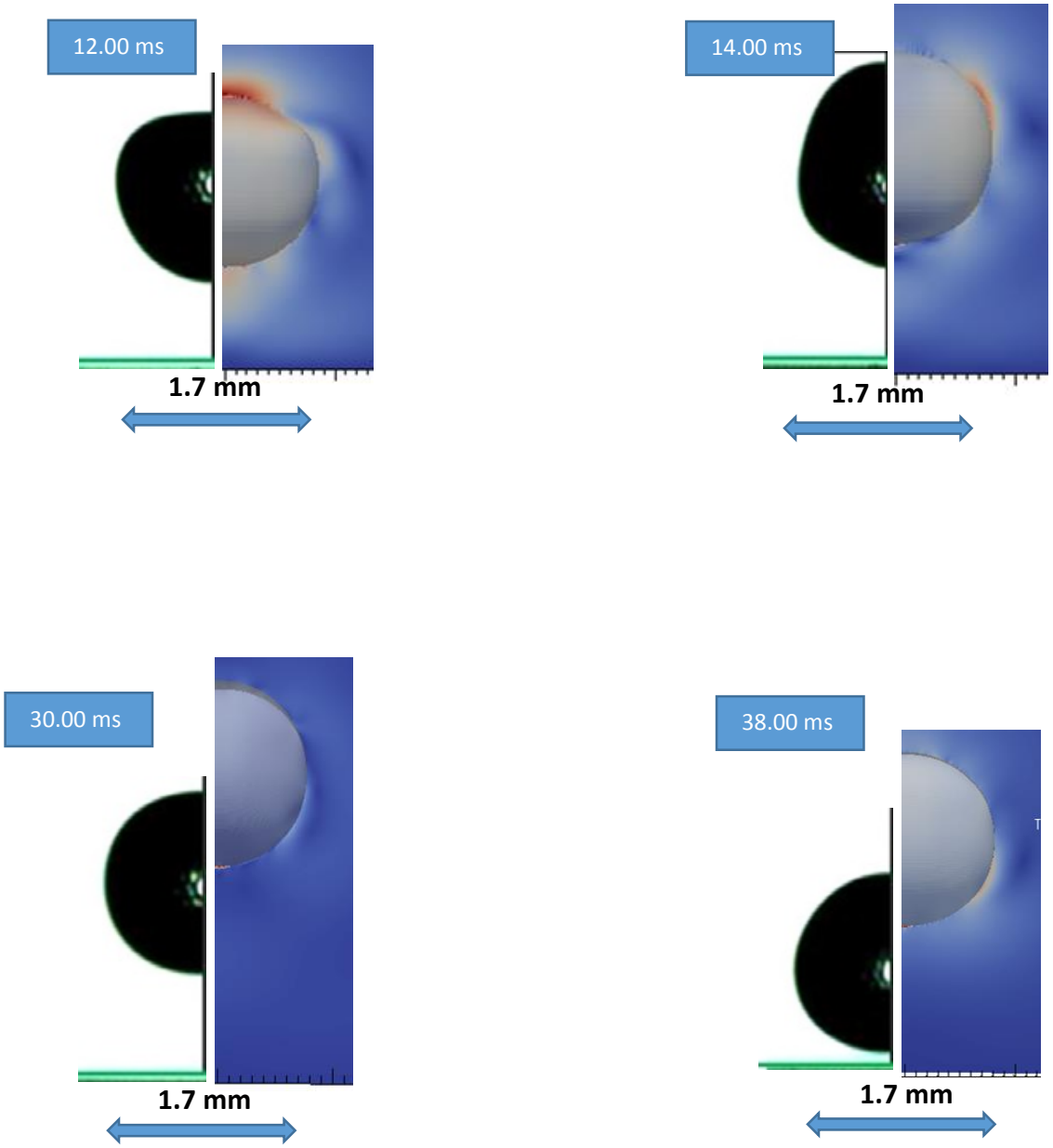

Figure 21: Comparison of Experiment's droplet shape (right side), with numerical simulations results of dynamicKistler' s model in different time periods (12.00 ms to 38 ms)

4.5.1 *Experiment IV*

Superhydrophobic and self-cleaning surfaces are of interest for various applications including self-cleaning windows, windshields, exterior paints for buildings and navigation of ships, utensils, roof tiles, textiles, solar panels and applications requiring antifouling and a reduction in drag in fluid flow, e.g. in micro/nanochannels. Bhushan et al. (2009) [7], did experiments of droplet impact on superhydrophobic nanostructured surfaces with a high static contact angle above 150° and contact angle hysteresis (the difference between the advancing and receding contact angles) below 10° exhibit extreme water repellence and self-cleaning properties (Bhushan & Jung (2008) [35], Nosonovsky & Bhushan (2008) [31], Bhushan et al. (2009) [32] . The Reynolds number (Re = $\frac{V_0 D_0}{\upsilon}$) is 880 and the Webber number(We = $\frac{\rho V_0 D_0^2}{\gamma}$) is 5.37. The diameter of the droplet is 2.0 mm and the impact velocity is 0.44 m/s. This experiment is also represented in Patil's et al. paper [7].

4.5.2 *Numerical results with respect of Experiment IV*

Comparison with experiment from Bushan et al. [7] with the dynamicKistler model of OpeFOAM are investigated in this case (Case 6) on a superhydrophobic surface. The number of cells is 1.6 million (1000 × 1600 × 1). In the directories of the OpenFOAM folders we used parameters as the experiment. We calculated those from the Re number (880) which is indicated in the Patil's et al. paper. The droplet diameter is 2.00 mm and the impact velocity of the droplet is 0.44 m/s.

4.5.3 Case 6

As the Case 5, only the dynamicKistlerAlphaContactAngle model of Case 6 will be compared with the experiment IV. The values of contact angles are, of θ_{eq}= 158°, θ_{Adv}= 165°, θ_{Rec}= 142°.

The following pictures are the numerical results of the Case 6 (right side), compared with photographs (left side) of the experiment by Bushan et al. [7]:

- Comparison of numerical results of Case 6 with the results of Experiment IV:

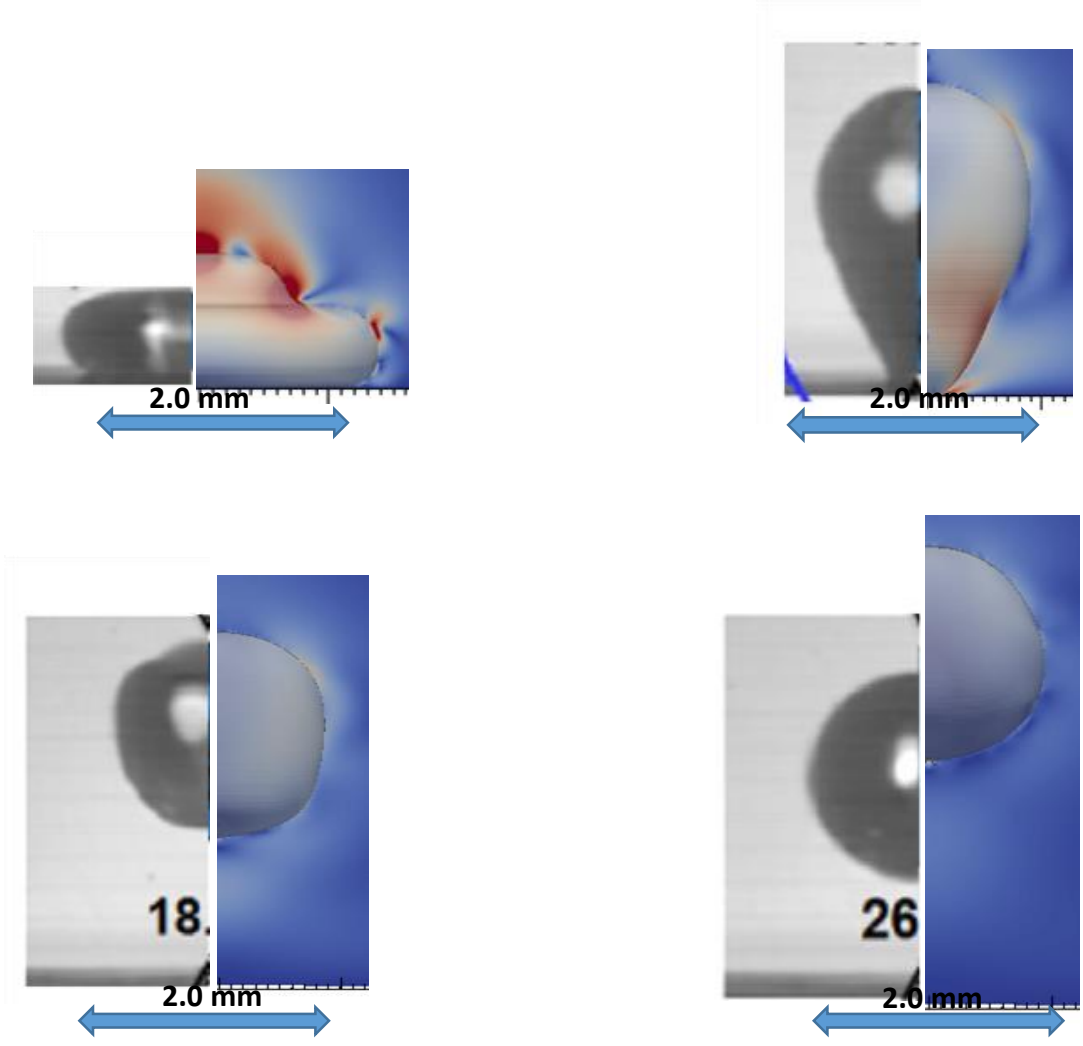

Figure 22: Spatial and temporal evolution of droplet after the time of impact, for four different time instances. Numerical (right) and experimental (left) snapshots.

4.5.4 *Comparison of the Experiment III and Numerical Results of CASE 6*

As we can see from the pictures above as well as from Graph 5, numerical and experimental results show very good agreement, not only in the shape of the droplet but also in the wetted diameter (before the detachment). Moreover, up to 18.20 ms, experimental and numerical results have similar time pace. However, in the experiment at the 26.20ms time period, the droplet has already started approaching the surface, on the other hand in the numerical simulation the droplet has just started falling towards the surface, resulting a small difference in the shape of the droplet as well as in the distance from the surface.

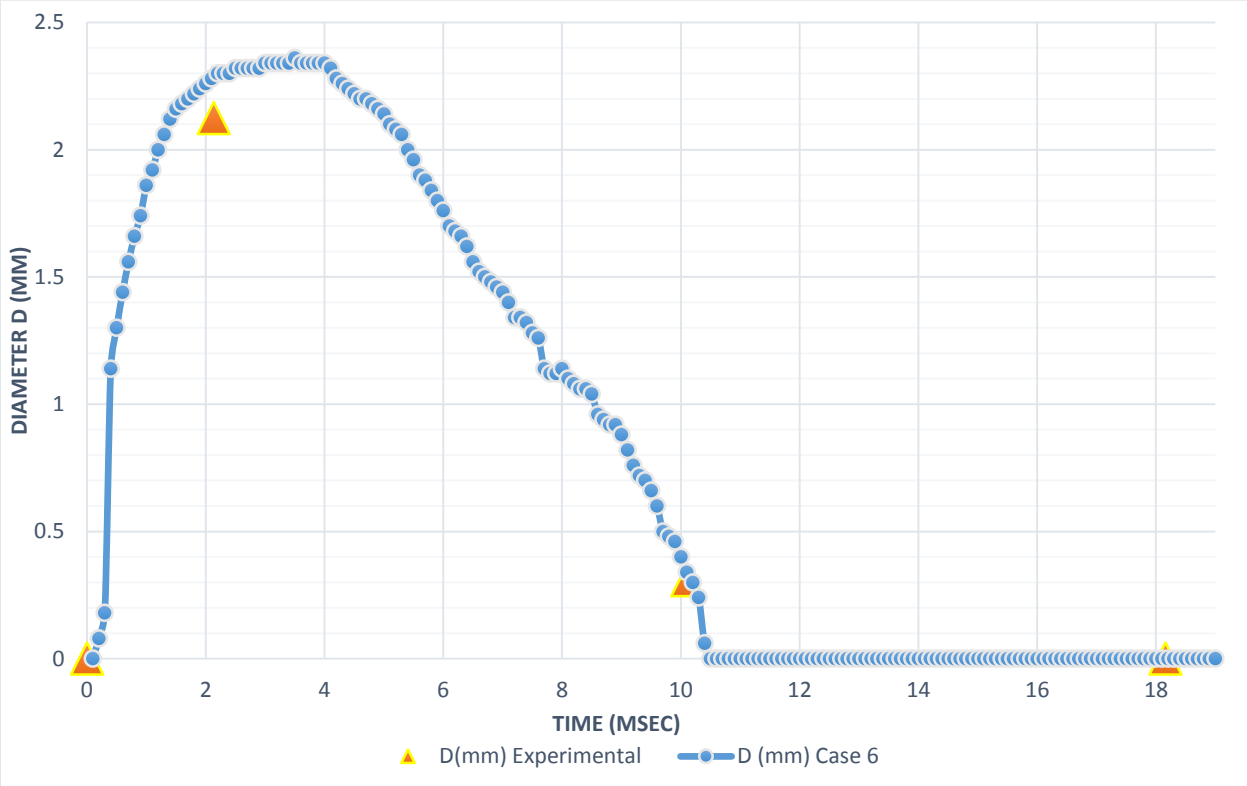

Graph 5: Comparisons of droplet's wetted diameter (D) of the Experiment IV, with dynamicKistler contact angle model

4.6.1 Conclusions

Investigation of 6 different numerical simulations have been conducted in this dissertation with a view to compare the numerical results with results from four different experiments available in literature [4] [5] [6] [7]. Using a user modified solver based on InterFOAM solver of OpenFOAM software. Two different contact angle models (Constant, Dynamic) of the official distribution of OpenFOAM and a new user-implemented model from the literature (Kistler) have been compared with experimental data. Comparing the three models the Dynamic contact angle model showed the less accurate results both in the shape as well as in the wetted diameter of the droplet. The Constant contact angle model showed more accurate results than the dynamic contact angle model (in many times it shows good agreement in shape as well as in the droplet's wetted diameter of the experiments). However, in most of the cases it gave bigger wetted maximum diameter Dmax. and in the recoiling phase it recoils faster that the droplets in the experiments. In the other hand, the dynamicKistler model showed the most accurate results comparing to the other two models, moreover comparing with the experimental result in most of the cases like, Case 4 and Case 6 (Figure 16 and 21) the maximum difference of the wetted diameter of the droplet was less than 0.2 mm (<0.2 mm).

5.1 References

[1] Kim J. Spray cooling heat transfer: The state of the art. Int. J Heat Fluid Flow 2007; 28 (4):753-67

[2] A. L. Yarin, "Drop impact dynamics: Splashing, spreading, receding, bouncing," Annu. Rev. Fluid Mech. 38, 159 2006.

[3] The physics of droplet impact on complex surfaces, Marco Marengo

[4] M. Pasandideh-Fard, Y. M. Qiao, S. Chandra, and J. Mostaghimi, "Capillary effects during droplet impact on a solid surface", Phys. Fluids 8 (3), March 1996

[5] Kensuke Yokoi, Damien Vadillo, John Hinch, and Ian Hutchings : Numerical studies of the influence of the dynamic contact angle on a droplet impacting on a dry surface, PHYSICS OF FLUIDS 21, 072102 (2009)

[6] Nagesh D. Patil, Vinesh H. Gada, Atul Sharma, Rajneesh Bhardwaj: On dual – grid level – set method for contact line modeling during impact of a droplet on hydrophobic and superhydrophobic surface, International Journal of Multiphase Flow 81 (2016) 54–66

[7] Bhushan ,B.,Jung, Y.C.,Koch , K., 2009. Micro-,nano- and hierarchical structures for superhydrophobicity, self-cleaning and low adhesion. Philos. Trans. R. Soc . A367, 1631–1672.

[8] Marco Marengo, Carlo Antonini, Ilia V. Roisman, Cameron Tropea : Drop collisions with simple and complex surfaces. Current Opinion in Colloid & Interface Science Volume 16, Issue 4, August 2011, Pages 292–30 (2012)

[9] Carlo Antonini, Alidad Amirfazli, and Marco Marengo : Drop impact and wettability: From hydrophilic to superhydrophobic surfaces, Phys. Fluids 24, 102104 (2012);

[10] Subhasish Mitra, Mayur J. Sathe, Elham Doroodchi, Ranjeet Utikar, Milin K. Shah, Vishnu Pareek, Jyeshtharaj B. Joshi, Geoffrey M. Evans : Droplet impact dynamics on a spherical particle, Chemical Engineering Science, Volume 100, 30 August 2013, Pages 105–119

[11] Monica Gumulya, Ranjeet P. Utikar, Vishnu Pareek, Ryan Mead-Hunter, Subhasish Mitra, Geoffrey M. Evans : Evaporation of a droplet on a heated spherical particle, Chemical Engineering Journal Volume 278, 15 October 2015, Pages 309–319

[12] Claas Willem Visser, Philipp Erhard Frommhold, Sander Wildeman, Robert Mettin, Detlef Lohse and Chao Sun : Dynamics of high-speed micro-drop impact: numerical simulations and experiments at frameto-frame times below 100 ns†, This journal is © The Royal Society of Chemistry 2015

[13] Ilias Malgarinos, Nikolaos Nikolopoulos, Marco Marengo, Carlo Antonini, Manolis Gavaises, "VOF simulations of the contact angle dynamics during the drop spreading: Standard models and a new wetting force model", Advances in Colloid and Interface Science 212 1–20 (2014)

[14] Zhong Zhang, Haifeng Liu, Fan Zhang, Mingfa Yao : Numerical study of spray micro-droplet impinging on dry/wet wall, Applied Thermal Engineering 95 (2016) 1–9

[15] A.Georgoulas, P. Koukouvinis, M. Gavaises, M. Marengo : Numerical Investigation of quasi-static bubble growth and detachment from submerged orifices in isothermal liquid pools: The effect of varying fluid properties and gravity levels, International Journal of Multiphase Flow 74 (2015) 59-78

[16] J.U. Brackbill, Douglas Ridge Kothe and C Zemach : A Continuum Method for Modeling Surface Tension, Article in Journal of Computational Physics · July 1992

[17] Hoang, D.A., van Steijn, V., Portela, L.M., Kreutzer, M.T., Kleijn, C.R., 2013. Benchmark numerical simulations of segmented two-phase flows in microchannels using the Volume of Fluid method. Comput. Fluids 86, 28–36. http://dx.doi.org/10.1016/j.compfluid.2013.06.024

[18] Deshpande, S.S., Anumolu, L., Trujillo, M.F., 2012. Evaluating the performance of the two-phase flow solver interFoam. Comput. Sci. Discov. 5, 014016. http://dx.doi.org/10.1088/1749-4699/5/1/014016.

[19] OpenFOAM, 2013. The OpenSource CFD Toolbox. User Guide. Version 2.2.1.

[20] A. Criscione, R. Rohrig, S. Jakirli´c, I. V. Roisman, C. Tropea : Impacting Droplets: Dynamic Contact Angle Modeling in OpenFOAM, 7th OpenFOAM®_ Workshop Center of Smart Interfaces, Technische Universitat Darmstadt, Germany 25 – 28 June 2012

[21] Sikalo, S., Wilhelm, H.-D., Roisman, I.V., Jakirli´c, S., Tropea, C., Dynamic contact angle of preading droplets: Experiments and simulations. In: Physics of Fluids, 17, 062103 (2005).

[22] Auro Ashish Saha, Sushanta K. Mitra : Effect of dynamic contact angle in a volume of fluid (VOF) model for a microfluidic capillary flow, Journal of Colloid and Interface Science 339 (2009) 461–480

[23] T.S. Jiang, S.G. Oh, J.C. Slattery, J. Colloid Interface Sci. 69 (1979) 74–77.

[24] Y.D. Shikhmurzaev, Capillary Flows with Forming Interfaces, Chapman & Hall/CRC, Boca Raton, 2008.

[25] Kistler, S.F., Hydrodynamics of wetting. In: Berg, J.C. (Editor): Wettability, Marcel Dekker, New York, 1993.

[26] A. Criscione, R. Röhrig, L. Opfer, I. Roisman and S. Jakirli´c Institute of Fluid Mechanics and Aerodynamics, Technische Universität Darmstadt, Petersenstraße 32, 64287 Darmstadt, Germany : Numerical investigation of impacting water drops in air cross, ILASS – Europe 2011, 24th European Conference on Liquid Atomization and Spray Systems, Estoril, Portugal.

[27] Roisman, I.V., Opfer, L., Tropea, C., Raessi, M., Mostaghimi, J., and Chandra, S., Drop impact onto a dry surface: role of the dynamic contact angle. In: Colloids and Surfaces A, Vol. 322, pp. 183-191 (2008).

[28] http://cfd.direct/openfoam/user-guide/blockmesh/ (Chris Greenshields, March 2015)

[29] Bhardwaj,R.,Attinger,D.,2008.Non-isothermal wetting during impact of millimeter-size water drop on a flat substrate : numerical investigation and comparison with high-speed visualization experiments . Int. J. Heat Fluid Flow 29, 1422–1435.

[30] Bhardwaj, R., Longtin, J.P., Attinger,D., 2010. Interfacial temperature measurements, high-speed visualization and finite-element simulations of droplet impact and evaporation on a solid surface . Int . J. Heat Mass Transf. 53, 3733–3744.

[31] Nosonovsky, M. & Bhushan, B. 2008b Roughness-induced superhydrophobicity: a way to design non-adhesive surfaces. J. Phys. Condens. Matter 20, 225009. (doi:10.1088/0953-8984/20/22/ 225009)

[32] Bhushan, B., Jung, Y. C. & Koch, K. 2009b Self-cleaning efficiency of artificial superhydrophobic surfaces. Langmuir 25, 3240–3248. (doi:10.1021/la803860d)